DESIGN OF A RE-USABLE ROCKET FOR TRIGGERED-LIGHTNING EXPERIMENTS

Michael David Grant

A dissertation submitted to the faculty of Engineering and the Built Environment, University of the Witwatersrand, in fulfilment of the requirements for the degree of Master of Science of Engineering.

Johannesburg, July 31, 2006

Declaration

I declare that this dissertation is my own, unaided work. It is being submitted for the Degree of Master of Science in the University of the Witwatersrand, Johannesburg. It has not been submitted before for any degree or examination in any other University.

.....

Michael David Grant

July 31, 2006

Abstract

This dissertation presents the design of a re-usable rocket for use in triggered-lightning experiments. It is intended that the rocket will tow a thin wire to sufficient height so that the lightning mechanism will attach onto the wire and follow it to ground. The rocket design is inherently safe as it does not use explosive materials for its propulsion system, and hence conforms to South African explosive legislation.

The designed rocket consists of a hybrid motor, which uses a solid combustion chamber and liquid oxidiser rather than solid motors which use a single solid fuel or a liquid motor which uses two liquid propellants. The mechanical performance of the oxidiser stage is critical in containing the pressurised oxidiser and regulating the flow of the oxidiser into the combustion chamber. The design of the combustion chamber and the rate at which the solid material burns is key to the generation of the pressure which is expelled through the nozzle to produce thrust. The design of the nozzle is covered in which the material from which it is made must withstand temperatures in excess of 1600 °C. The entire system was modelled to calculate the parameters of the various subsystems. The simulation study shows that the rocket will be able to reach 1 km with a complete section of wire towed behind it.

A cost analysis, against other commercial rocket systems, was performed. The analysis concludes from the total cost of ownership that it is significantly cheaper to operate the designed rocket, over the course of the experiment, than other rocket systems.

Acknowledgments

Special thanks need to be extended to Mr. K. Nixon, whose engineering supervision possessed great enthusiasm and critical analysis. His awareness of the larger picture while focussing on specific issues provided valuable guidance.

In no particular order: Harry Fellows, EIE Workshop; Darren Osthuizen, Hyfit Expertek cc; Stuart Ratcliff and Kevin Ewels, Air Traffic Navigation Services; Andrea Ehmke, Armando De Olim, Bruce Paull, Mauritz Van Heerden South African Air Force; Randall Paton, Aeronautical Engineering; Ronald Armitage, Standerton Test Range.

For their invaluable input: Andrew Swanson, Miguel Fernandes, Andrew Spottiswoode, Andrew Dickson, Simon Hoffe, Joanne Garrard.

This work is dedicated to my parents who gave me every chance at success, and the encouragement to seize it.

Mariana, thank you for the support through difficult times.

To my colleagues for their support, encouragement, interest and criticism.

To strive, to seek, to find, and not to yield.
–Alfred Tennyson

Contents

List of Figures

List of Tables

List of Symbols

h	Height of rocket [m], *Equation (1), pg 5.*
E	Electric-field magnitude [kV/m], *Equation (1), pg 5.*
σ_h	Hoop Stress [Pa], *Equation (2), pg 6.*
P	Pressure inside vessel [Pa], *Equation (2), pg 6.*
r	Outer radius of tube [m], *Equation (2), pg 6.*
w	Thickness of tube [m], *Equation (2), pg 6.*
$\dot{m}_o$	Mass flow rate [kg/s], *Equation (3), pg 7.*
C	Discharge co-efficient, *Equation (3), pg 7.*
A_t	Injector cross-sectional area [m^2], *Equation (3), pg 7.*
ρ_o	Fluid density [kg/m^3], *Equation (3), pg 7.*
Δp	Differential pressure across nozzle [Pa], *Equation (3), pg 7.*
γ	Area expansion ratio, *Equation (3), pg 7.*
R	Radius of combustion chamber [m], *Equation (4), pg 8.*
a	Regression rate co-efficient, *Equation (4), pg 8.*
t	Time from combustion start [s], *Equation (4), pg 8.*
n	Regression rate exponent, *Equation (4), pg 8.*
R_i	Initial radius of combustion chamber [m], *Equation (4), pg 8.*
$\dot{m}_f$	Rate of fuel formation [kg/s], *Equation (5), pg 8.*
ρ_f	Density of solid phase [kg/m^3], *Equation (5), pg 8.*
L	Length of solid phase [m], *Equation (5), pg 8.*
$\mathcal{P}$	Rate of Energy transfer [W], *Equation (6), pg 8.*
k_T	Thermal conductivity constant [W/K], *Equation (6), pg 8.*

A_h Surface area exposed to head [m^2], *Equation (6), pg 8.*

dT/dx Thermal gradient [K/m], *Equation (6), pg 8.*

C_t Specific heat capacity [W], *Equation (7), pg 8.*

V Volume of material [m^3], *Equation (7), pg 8.*

c Specific heat [W/kg], *Equation (7), pg 8.*

v_e Exhaust velocity [m/s], *Equation (8), pg 9.*

k Specific heat ratio, *Equation (8), pg 9.*

$\mathcal{R}$ Gas constant per unit weight [J/kg·K], *Equation (8), pg 9.*

T Absolute temperature of the gas [K], *Equation (8), pg 9.*

p_e Exhaust pressure [Pa], *Equation (8), pg 9.*

p_c Chamber pressure [Pa], *Equation (8), pg 9.*

v_c Inflow velocity [m/s], *Equation (8), pg 9.*

F Force [N], *Equation (9), pg 9.*

$\dot{m}$ Mass flow of material [kg/s], *Equation (9), pg 9.*

p_n Nozzle throat pressure [Pa], *Equation (9), pg 9.*

p_e Exhaust gas pressure [Pa], *Equation (9), pg 9.*

A_n Nozzle cross-sectional area [m^2], *Equation (9), pg 9.*

σ_a Axial stress [Pa], *Equation (3), pg 20.*

p_1 Combustion chamber pressure [Pa], *Equation (2), pg 26.*

c^* Chamber characteristic velocity [m/s], *Equation (2), pg 26.*

g_0 Gravity [m/s^2], *Equation (2), pg 26.*

c_p Specific heat at constant pressure [J/kg·K], *Equation (4), pg 29.*

c_v Specific heat at constant volume [J/kg·K], *Equation (4), pg 29.*

J Mechanical equivalent of heat, $J = 4.186$ [J/cal], *Equation (4), pg 29.*

v_s Speed of sound [m/s], *Equation (6), pg 29.*

T_0 Stagnation temperature of gas [K], *Equation (8), pg 30.*

F Force [N], *Equation (13), pg 31.*

I - Introduction

Research into the natural lightning phenomenon is restricted to the chaotic distribution of lightning strikes over the surface of the earth. It was Franklin who first noted that lightning was more prone to striking a taller structure that the surrounding area [1]. Lightning research is limited in this area as tall structures are expensive to erect; and are often used for more critical applications [2].

If it were possible to bias the lightning phenomenon to strike a particular point, with little interference from surrounding topography, then further research could be facilitated. Rockets, trailing earthed wires, were first fired into thunder clouds from ships off the Florida coast in the early 1960's [1, 3]. If timed correctly, the leader mechanism attaches to the tip of the rocket; thus completing a path down which the main strike current can flow and effectively triggering a lightning strike.

Currently research through rocket triggered-lightning studies is being done in the United States of America by two teams: the first based at the International Center for Lighting Research, Camp Blanding, Florida [4]; and the second at the New Mexico Institute of Mining and Technology, in Langmuir, New Mexico. Triggered lightning studies have also been done in Japan, where it is mostly winter lightning that they experience [5].

Rocket triggered-lightning has since proven to be a valuable method of investigating the phenomenon [1, 3, 4]. The method has provided insights into the mechanism which produces the ionised channel along which the strike current flows; and into the secondary effects of the phenomenon such as interference caused by the radiation from the charge transfer [4]. Practically, this improved understanding is used to better equip industry to protect against the deleterious effects of the lightning phenomenon.

South African legislation is very restrictive as to the production and use of explosive materials, under which solid rocket propellant is categorised [6]. The Acts forbid the following without several costly licenses:

- Manufacture of any explosive material.
- The ignition of any explosive material.

In developing a platform from which to conduct rocket triggered-lightning studies, the rocket presented in this design was created. The decision to launch the rocket to trigger lightning is based on an incident electric field measurement. The electric field increases as the lightning leader mechanism approaches earth; and studies have shown that for electric fields above 4 kV/m, there is a 95% chance of triggering lightning with the described rocket methods.

The electric field sensor, in the form of an electric field mill, is able to detect the magnitude of the incident electric field. This sensor has already been designed, tested and presented elsewhere, but has been included as an appendix for completeness [7].

Problem statement

Given the large number of rocket launches required in order to conduct a thorough triggered-lightning study and the fact that any solid fuel motor would have to be imported, another means of firing rockets was sought. The hybrid rocket motor, which is the synthesis of solid and liquid fuel models, is appealing because it can be designed with stages (liquid and solid) which are not classed as explosive material. The hybrid rocket motor design also presents an inherent element of safety as most failures result in the extinguishing of the combustion process; a fallback most certainly not present in either of the other two motor models [8].

In order to facilitate the triggered-lightning experiments a hybrid rocket has been engineered to meet the following specifications

1. Tow a thin copper wire to 1 km.
2. Inherently safe to manufacture and operate.
3. Re-usable.
4. Cheap to manufacture and operate.

Initially the hybrid rocket motor was simulated, through which the various parameters calculated and materials determined. An initial prototype engine was then constructed and rigorously tested. Modifications on the initial design were then made, re-simulated and finally tested. It is this modified design that is presented in the paper.

The format of this dissertation differs from that of a conventional dissertation in that it is a short paper, followed by a number of appendices. The paper is complete and details the design, models and solution obtained; however for more in depth explanations and calculations please refer to the appropriate appendix.

Paper: In a short paper format the design of the hybrid rocket is presented. The paper covers the various design parameters of the hybrid motor, ignition system, construction requirements, aerodynamic considerations and an economic analysis. The paper has a separate set of references from the rest of this document. This paper is a revised version of one that has been accepted for publication in the proceedings of the 28^{th} International Conference on Lightning Protection, Kanazawa, Japan [9].

Appendix A - Oxidiser stage design: This section presents a detailed discussion of the various parameters of the oxidiser (liquid) stage of a hybrid rocket motor. It forms the framework from which the behaviour of the liquid stage can be simulated.

Appendix B - Combustion stage design: This section presents a detailed discussion of the various parameters of the combustion (solid) stage of the hybrid design. The section details how the behaviour

of this stage depends on both the physical properties of the chamber and the flow of liquid oxidiser into it.

Appendix C - Nozzle design: This section presents the design of the nozzle used on the hybrid rocket. It determines how the combustion chamber pressure and specific mass velocity of the combustion products are transformed into thrust. It completes the framework from which an accurate simulation study can be performed.

Appendix D - Simulation model: The simulation model from which the behaviour of the rocket motor was predicted is presented in this section. It uses the framework provided by appendices A, B and C and ultimately predicts the apogee of the rocket's flight.

Appendix E - Launch system design: The mechanical design of the launch rail and interface onto the rocket is presented in this section. As the rocket has no active guidance, it needs to accelerate sufficiently before leaving the launch rail so that the static fins have enough influence to ensure straight flight.

Appendix F - Project expenditure: The project bill of materials and prototyping costs are presented for reference.

Appendix G - Technical drawings: A complete set of technical drawings from which the rocket can be constructed are presented in this appendix. Materials, dimensions and tolerances are as indicated.

Appendix H - Electric Field Mill: This paper was presented at the 2006 SAUPEC conference. It details the design, construction and operation of an electric field mill that is capable of detecting pre-strike conditions.

DESIGN OF A RE-USABLE ROCKET FOR TRIGGERED-LIGHTNING EXPERIMENTS

Michael D. Grant
School of Electrical and Information Engineering,
University of the Witwatersrand, Johannesburg, South Africa.

***Abstract* – The design of a re-usable hybrid rocket for use in triggered-lightning experiments is presented. The fuel tank and combustion chamber behaviour is analysed, as is a thrust model for rocket performance prediction. Finally a cost analysis is performed against available solid fuel rocket motors and it is found that the hybrid rocket is significantly cheaper to operate over the number of launches expected in the triggered-lightning study.**

***Keywords*– hybrid fuel; re-usable rocket; rocket design; total cost of ownership; triggered-lightning.**

1 Introduction

Given the inherent complexity of the stepped leader mechanism which, by and large, is responsible for the formation of the ionised channel along which the majority of charge transfer occurs; it is challenging to conduct a rigourous study of the lightning phenomenon.

However if it were possible to bias the discharge to a specific point, then the characteristics of lightning could be studied. And indeed it is possible: high towers with large collection areas can be instrumented; large areas can be covered with small towers; and lightning can be artificially triggered [1, 2].

Revised version of paper accepted for publication in 28th International Conference on Lightning Protection, Kanazawa, Japan [3]

1.1 Triggered-Lightning

There are two proposed methods of triggering lightning, both of which involve replacing the leader mechanism with a conductive channel between the cloud and ground: it might be possible to use a laser to ionise an intermediate channel, thus creating conditions similar to that just after the attachment mechanism has completed [4]. However this mechanism has yet to progress out of the laboratory although initial results are promising. The only other means involves the launch of a small rocket trailing a wire.

In classical rocket triggered-lightning the wire between the rocket and ground is continuous and the rocket remains at earth potential. In altitude triggered-lightning the rocket simply trails the wire and biases the strike towards a strike point. The two different rocket triggering methods yield differing characteristics in the initial strike current [5].

Lightning strike prediction can be performed from ground based electric field measurements. This is easily achieved with inexpensive devices such as a field mill [6]. Thus the decision to launch a rocket to trigger lightning is based on the electric field measurements using the correlation between the electric field magnitude and the height a rocket has to fly before attaching to a downward leader, found by Hubert *et al.* [5]:

$$h = 3900E^{-1.33} \quad (1)$$

Where:
h : Height of rocket [m]
E : Electric-field magnitude [kV/m]

1.2 Rocket Flight

Small model rockets are ideally suited to tow short sections of thin wire to suitable height in order to trigger lightning. They most often consist of a single use solid fuel motor encased inside an aerodynamic body.

South African regulations make the ownership and use of solid rocket fuels prohibitive as a large number of expensive licenses are required [7]. Additionally there is no local source of solid rocket motors and hence the motors would have to be imported. Local fabrication of explosive material in the volumes required for a model rocket is illegal [7]. Combined, the cost per launch is so large that it is not feasible to conduct a thorough rocket triggered-lightning study.

Instead a low cost rocket capable of triggering lightning has been designed which conforms to the explosives control act, and is economically viable. In addition this type of combustion produces fewer toxic by-products and places a lower environmental load on the test facility.

2 Rocket Design

There are three distinct types of fuels used in combustion rockets: solid, liquid and hybrid. Solid fuel motors consists of a single substance which is a mixture of fuel and oxidiser, and is chemically unstable. Once ignited the rate of combustion cannot be regulated and typically increases with chamber pressure which can result in serious explosions [8].

Liquid fuel rocket motors consist of two liquid substances which are combined in the combustion chamber and combustion is regulated by adjusting the mass flow rates of either of the pressurised liquids [9]. Liquid fuel rocket motors are far too mechanically complex to implement in the scale required.

Rocket motors based on hybrid fuels consist of a solid fuel and liquid oxidiser and have a higher specific impulse than liquid fuels, but less than solid fuels; the combustion rate in hybrid motors is controlled by regulating the mass flow rate of the liquid oxidiser [10].

The presented design is based on the hybrid fuel model, and uses polypropylene for the solid fuel grain, and nitrous oxide for the oxidiser. Independently both substances are non-explosive; and their combination is not explosive provided that the surface temperature of the polypropylene is less than the degradation point of the polymer (286°C) [11]. These features are integral to the safety of the rocket design presented.

2.1 Liquid Phase

The liquid gas in the oxidiser tank is nitrous oxide (N_2O). *Figure 2* illustrates that the oxygen atom has the weakest bond in the molecule and thus the oxygen is easily liberated. Chemically this structure translates to a potent oxidiser; however when compared with other liquid oxidisers like liquid oxygen, N_2O is much simpler and safer to implement although less potent [12].

With reference to *Figure 1*, the portion of the rocket between the pressure cap and the piston

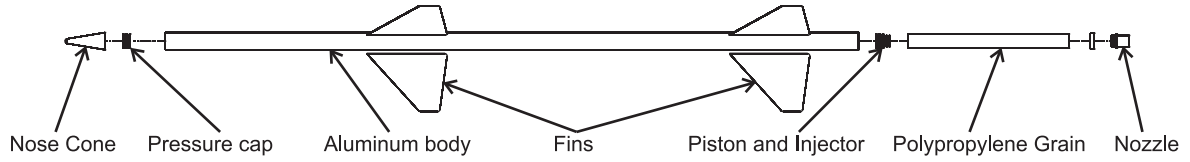

Figure 1: Diagram of hybrid rocket showing nose cone, pressure cap, body, fins, piston injector, fuel grain and nozzle

$$N \equiv N^+ - O^- \longleftrightarrow N^- = N^+ = O$$

Figure 2: Molecular structure of nitrous oxide

injector is filled with pressurised liquid N_2O. This is achieved by placing the rocket vertically and displacing the gas in the pressure vessel section with liquid N_2O from below. Practically this is achieved by feeding the liquid N_2O into the pressure chamber through nylon tubing through the nozzle and combustion chamber. The gas can escape through a gas jet in the pressure cap.

Nitrous oxide, at standard temperature, is liquid at pressures greater or equal to the vapour pressure of the oxidiser (see *Table 1* [13]). By venting gas through the gas jet at the top of the pressure vessel energy is removed from the system and the temperature of the liquid drops. Thus the pressure inside the vessel will settle to the vapour pressure.

Table 1: Table of nitrous oxide physical properties

Vapour pressure (20°C)	5.85 MPa
Liquid density	1222.8 kg/m^3
Critical temperature	36.4°C
Critical pressure	7.24 MPa

The pressure inside the vessel translates to axial and radial expansion. The axial stress, or force causing elongation along the axis of the cylinder, can be neglected because the surface area on the cap and piston is much smaller in comparison to the surface area of the tube. The radial expansion, called the Hoop stress, is the tangential sheer stress realised around the loop of the pressure vessel and is given by the equation:

$$\sigma_h = \frac{Pr_o}{w} \tag{2}$$

Where:
σ_h : Hoop Stress [Pa]
P : Pressure inside vessel [Pa]
r_o : Outer radius of tube [m]
w : Thickness of tube [m]

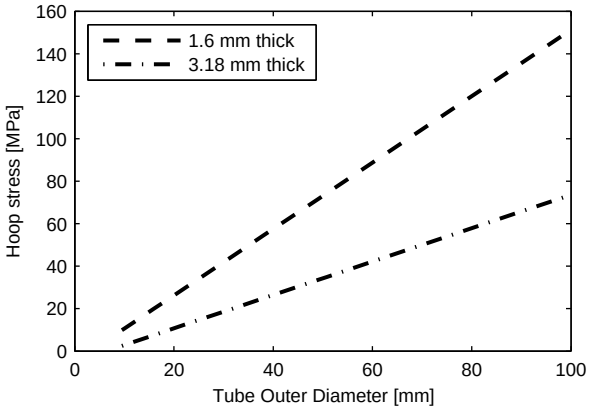

Figure 3: A comparison of Hoop stresses for two thickness tubes and varying external diameters at a nominal internal pressure of 5 MPa

A comparison is shown in *Figure 3*, obtained using the data in *Table 2* [14]. For a tube with an external diameter of 38.1 mm and a wall 1.6 mm

thick, this yields a maximum internal pressure of 13.5 MPa for the vessel, a safety margin of 100% above the expected vapour pressure.

Table 2: Table of aluminium alloy 6063-T6 properties

	Min	Typ	Max
Tensile Strength (MPa)	185	215	245
Proof Stress (MPa)	160	205	-

The liquid oxidiser is injected into the combustion chamber through a nozzle. The rate at which liquid gas flows through a constriction with a pressure differential is given by [15]:

$$\dot{m}_o = \frac{CA_t\sqrt{2\rho_o\Delta p}}{\sqrt{1-\gamma^2}} \tag{3}$$

Where:
$\dot{m}_o$: Mass flow rate [kg/s]
C : Discharge co-efficient
A_t : Injector cross-sectional area [m^2]
ρ_o : Fluid density [kg/m^3]
Δp : Differential pressure across nozzle [Pa]
γ : Area expansion ratio

Since the mass of oxidiser can be calculated from the volume of the pressure vessel and density of the pressurised liquid, and the vapour behaviour of the pressurised liquid; the combustion rate can be designed for by adjusting the parameters of the injection nozzle as described by *Equation 3*. The behaviour can be accurately modelled and is illustrated in *Figure 4*.

2.2 Solid Phase

The solid phase of the hybrid motor is made from polypropylene, and since combustion occurs on the surface of the plastic this stage is also known as the combustion chamber [10, 16].

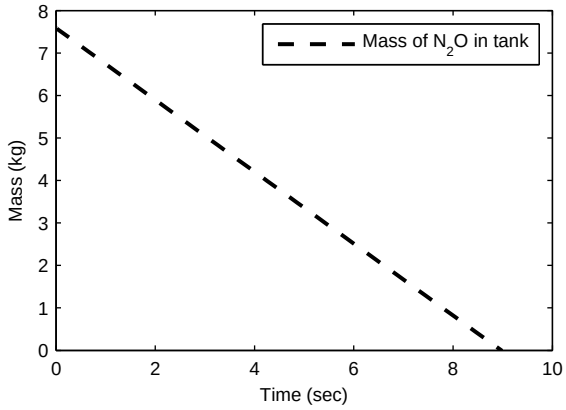

Figure 4: Simulated mass of remaining liquid nitrous oxide over time

Table 3: Table of polypropylene combustion properties

Regression rate exponent	0.65
Regression rate co-efficient	0.015
Melting point	173°C
Degradation point	286°C
Thermal conductivity	0.12 W/m·K
Specific heat	1750 J/K·kg

Optimisation of the surface area of the chamber is vital for efficient combustion of the combined fuels. However the introduction of complex surface patterns drastically increases the cost of production. By keeping the pattern simple, that of a cylinder, but maximising the inner radius, sufficient surface area for combustion is provided.

Now as combustion progresses the diameter of the combustion chamber increases since plastic on the surface is used as fuel. This regression rate is dependent on the mass of oxidiser flowing into the chamber and the rate at which the plastic combusts. The radius of the chamber is given by [10]:

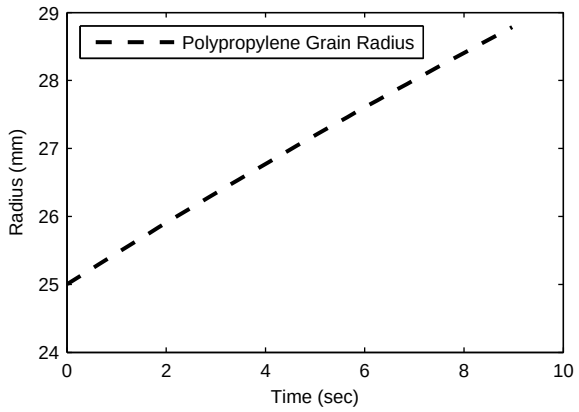

Figure 5: Simulated regression of solid fuel grain during combustion

$$R(t) = \left(at(2n+1)(m_o/\pi)^n + R_i^{(2n+1)}\right)^{1/(2n+1)} \tag{4}$$

Where:
R : Radius of combustion chamber [m]
a : Regression rate co-efficient
t : Time from combustion start [s]
n : Regression rate exponent
R_i : Initial radius of combustion chamber [m]

The application of the liquid oxidiser onto the combusting polypropylene causes "fuel" to form within the combustion chamber. The rate by which fuel is formed is given by [10, 12]:

$$\dot{m}_f = 2a\pi^{1-n}\rho_f L(m_o^n)R^{1-2n} \tag{5}$$

Where:
$\dot{m}_f$: Rate of fuel formation [kg/s]
a : Regression rate co-efficient
n : Regression rate exponent
ρ_f : Density of solid phase [kg/m^3]
L : Length of solid phase [m]
R : Radius of combustion chamber [m]

Since the regression constants of polypropylene have been determined experimentally and the behaviour of the oxidiser injection system can be accurately modelled it is possible to predict the regression behaviour of the combustion chamber, as illustrated in *Figure 5* [11, 12, 17].

Since the chamber is within the aluminium body of the rocket, the body needs to be thermally insulated from the heat generated within the chamber. If regression progresses too far and burns through the polypropylene onto the wall of the rocket, the aluminium will most probably fail under the pressure and temperature. To avoid this, and provide the required insulation, the thickness of the polypropylene chamber is increased to provide a safety margin of 85%, or 6mm.

The rate at which energy is transferred through the polypropylene is given by [18]:

$$\mathcal{P} = k_T A_h \frac{dT}{dx} \tag{6}$$

Where:
$\mathcal{P}$: Rate of Energy transfer [W]
k_T : Thermal conductivity constant [W/K]
A_h : Surface area exposed to head [m^2]
dT/dx : Thermal gradient [K/m]

The amount of heat energy that the polypropylene can absorb termed the specific heat capacity is given by [15, 18]:

$$C_t = \rho_f V c \tag{7}$$

Where:
C_t : Specific heat capacity [W]
ρ_f : Density of solid phase [kg/m^3]
V : Volume of material [m^3]
c : Specific heat [W/kg]

Thus the heat transfer from the combustion chamber to the aluminium body is modelled by a first order step response, where the time constant is

given as $\tau = 1/(kA_hC)$. Designing for the maximum burn time, expected chamber temperature and the addition of a safety margin will ensure that the temper of the aluminium body is not stressed.

2.3 Nozzle and Thrust Model

The exhaust velocity of the gasses out of a nozzle for a given inflow velocity is:

$$v_e = \sqrt{\frac{2k}{k-1}\mathcal{R}T\left[1-\left(\frac{p_e}{p_c}\right)^{(k-1)/k}\right]+v_c^2} \quad (8)$$

Where:

v_e : Exhaust velocity [m/s]
k : Specific heat ratio
$\mathcal{R}$: Gas constant per unit weight [J/kg·K]
T : Absolute temperature of the gas [K]
p_e : Exhaust pressure [Pa]
p_c : Chamber pressure [Pa]
v_c : Inflow velocity [m/s]

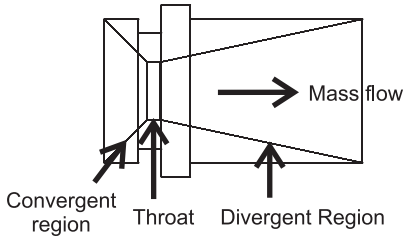

Figure 6: Rocket nozzle showing the convergent, throat and divergent regions, given the mass flow direction

The vapour pressure of the fuel tank is expected to be the maximum pressure exerted by the gas onto the combustion chamber and hence the maximum combustion chamber pressure must not exceed this. The introduction of a safety margin to this pressure will ensure that there is no back burn into the liquid gas chamber.

The change in thrust during the flight of the rocket through 1000 m due to variance in atmospheric pressure is less than 2% [10, pg 68], and this term is removed for simplification. Thus the thrust of the rocket, given the supersonic mass flow of combustible material, and the properties of the nozzle is given by [10]:

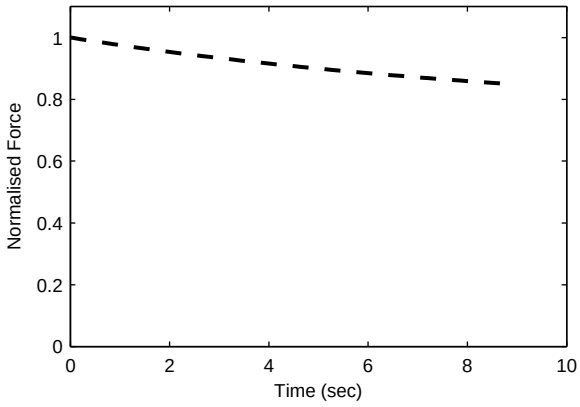

Figure 7: Normalised thrust of hybrid rocket motor for burn duration

$$F = \dot{m}v_e + (p_n - p_e)A_n \quad (9)$$

Where:

F : Force [N]
$\dot{m}$: Mass flow of material ($\dot{m} = \dot{m}_o + \dot{m}_f$) [kg/s]
p_n : Nozzle throat pressure [Pa]
p_e : Exhaust gas pressure [Pa]
A_n : Nozzle cross-sectional area [m^2]

2.4 Ignition and Launch

The rocket is ignited by a small block of solid fuel propellant which burns within the combustion chamber. This heats the surface of the polypropylene to the degradation temperature and then severs the N_2O feed line starting the burn of the rocket motor.

The solid fuel igniter is made from potassium nitrate (KNO_3) and sucrose. The ratio of 65% KNO_3 to 35% sucrose has been experimentally

determined to yield the fastest burning rate [8]. The solid fuel block is made by carefully mixing the two chemicals above an isolated heat source. It is important to note that this mixture is explosive and chemically unstable and therefore should not be exposed to excessive heat.

The ignition can be started by applying a small amount of concentrated heat to the solid fuel igniter: this is achieved by wrapping a strip of resistive wire ($\rho = 1.5$ kΩ/m) around the solid fuel block and then driving current through the resistive strip.

The solid fuel igniter must burn from the outside; so that the surface of the combustion chamber is well into a burn phase before the cold and potentially extinguishing liquid N_2O is released into the chamber.

2.5 Construction Requirements

The body of the rocket is made from a tube of aluminium with a circlip groove cut into the inner surface of the tube near each end. These grooves are easily cut into the tube with a lathe. The pressure cap and piston-injector parts are made from aluminium rod and fit into the body. Grooves to hold O-rings to seal the liquid phase are cut into each. The cuts are simple and can also be done with a lathe.

The combustion chamber can be made from either a section of polypropylene rod or tube. If a tube of polypropylene is used, then the inner radius must adhere to the design constraints presented previously. The tube can also be turned on a lathe so that it fits into the body of the rocket.

It is preferable that the fins are laser cut out of aluminium sheet 0.7 mm thick, and then bent to the profile required; the fins can then be attached onto the body with epoxy resin.

3 Aerodynamic Factors

The wind resistance experienced by the rocket is proportional to the cross-sectional area of the rocket. Similarly the drag from the rocket is also proportional to the cross-sectional area of the rocket.

The maximum free-flight velocity can be estimated from the thrust model and frictional forces, and is simulated at Mach 3, or 900 m/s. The maximum velocity will be reduced when the rocket is trailing a wire.

3.1 Flight Stability

The rocket requires some means of ensuring vertical flight without the overheads of additional avionics; protecting the electronics from the expected interference of the lightning channel is complex and defeats the objectives of the project. The addition of static fins placed normal to the body are sufficient to ensure stable flight.

However the cross sectional area of the fins is too small to counter any deflections that the rocket might experience at low wind speeds. This is solved by launching the rocket off a rail, which is long enough to ensure sufficient acceleration of the rocket before left to the passive guidance of the fins.

4 Electronics

The rocket is equipped with a dipole antenna that runs the length of the rocket.

Realistically it is expected that a maximum tracking range will be one kilometre, with 40% extra to ensure recovery of the rocket. During flight the dipole is shorted to the body of the rocket with a relay to protect the transmitter from over voltages due to the lightning current.

5 Economic Analysis

Since the emphasis of the design is that of low cost, the total cost of ownership (TCO) of the triggered-lightning experiments is important. Provided that the experiments are conducted over a short interval, long term economic effects like inflation can be ignored.

It should be noted that while the initial costs of the hybrid rocket system are larger, the TCO of both systems is the same after 18 launches. Beyond that point, the hybrid system is significantly cheaper: with each launch costing 45% less.

The startup cost for the hybrid rocket is ZAR 1300 and consists of:

1. Raw materials for the rocket.
2. Labour costs.
3. Construction materials.
4. Re-usable launch items.

The cost of each launch of the hybrid rocket is ZAR 103.5 and consists of:

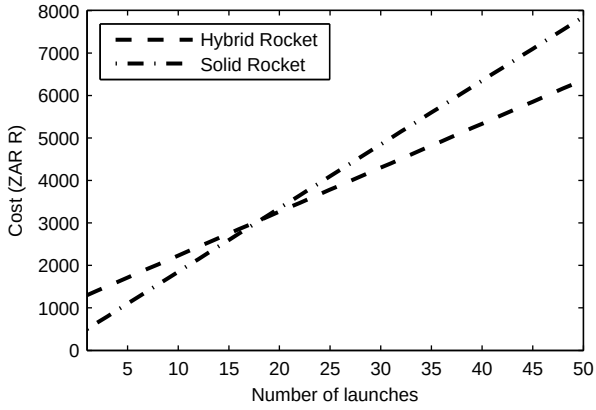

Figure 8: Total cost of ownership vs. number of launches for Hybrid and Solid fuel rockets

1. Liquid N_2O used.
2. Polypropylene combustion chamber.
3. Solid fuel igniter.
4. Feed piping.

The startup cost of available model rocket systems is in the region of ZAR 500.00; the cost consists of the same items except that no labour or construction materials are required. The fact that these models are mass produced reduces the cost further.

The cost per launch of solid fuel rockets simply consists of the solid fuel motor which is not re-usable. The retail price for a solid fuel motor that produces equivalent thrust to the designed hybrid rocket is ZAR 150.00

South African law requires a license to fire solid fuel rocket motors which costs ZAR 120.00, but this additional cost has been excluded from the startup cost of the available model rocket systems as it is not globally applicable.

6 Discussion

The rocket design presented in this paper has been constructed and tested. Several static tests were conducted, from which the ignition system and nozzle design was improved. The performance of the nozzle was found to be adequate as Mach diamonds were sighted [10]. Free flights have also been done and the launch rail and ignition system tested.

7 Conclusion

The design of a hybrid rocket that conforms to South African explosive legislation is presented and analysed. The behaviour of the individual components of the rocket are presented as well as their combined response in order to model the rocket's behaviour. The ignition process and materials along with aerodynamic considerations have been presented.

Finally the total cost of ownership versus available model rockets is analysed, and finds that the hybrid system is significantly cheaper to operate. The financial implications of performing a through study are reduced by using the most economical solution.

References

[1] V. Rakov, M. Uman, and K. Rambo. A review of ten years of triggered-lightning experiments at Camp Blanding, Florida. *Journal of Atmospheric Research*, vol. 76, pp. 503–517, 2005.

[2] B. Kordi, R. Moini, W. Janischewskyj, A. Hussein, V. Shostak, and V. Rakov. Application of antenna theory model to a tall tower struck by lightning. *Journal of Geophysical Research*, vol. 108, no. D17, pp. 7.1–7.9, 2003.

[3] M. D. Grant and K. J. Nixon. Design of a re-usable rocket for triggered-lightning experiments - Paper 1363., Sep. 2006. Accepted for publication at the *28^{th} International Conference on Lightning Protection* Kanazawa, Japan.

[4] N. West, I. R. Jandrell, and A. Forbes. Preliminary investigation into laser-high voltage interaction in the case of the streamer-to-leader process using high power CO_2 lasers., Sep. 2006. Accepted for publication at the *28^{th} International Conference on Lightning Protection* Kanazawa, Japan.

[5] V. Rakov and M. Uman. *Lightning: Physics and Effects*. The Edinburgh Building, Cambridge CB2 2RU, England: Cambridge University Press, 2003.

[6] M. D. Grant, J. Garrard, and K. J. Nixon. Low cost electric-field mill: Design, Construction and Testing. In *Proceedings of the 2006 Southern African Universities Power Engineering Conference*. Durban, South Africa, Jan. 2006.

[7] Acts Online - South African Hypertext Legislation. Internet: http://www.acts.co.za, September 2005.

[8] A. Vyverman. Simulation of Potassium Nitrate-Sugar Rocket Motors. *Vlaamse Raket Organisatie (Flemish Rocket Organisation)*, 2002.

[9] C. Kuhl, H. Wright, C. Hunter, C. Guernsey, and A. Colozza. Liquid Rocket Propulsion for Atmospheric Flight in Proposed ARES Mars Scout Mission. *American Institute of Aeronautics and Astronautics*, 2004.

[10] G. Sutton and O. Biblarz. *Rocket Propulsion Elements*. Wiley-Interscience, 7 ed., 2000.

[11] M. Wey and C. Chang. Kinetic study of polymer incineration. *Polymer Degradation and Stability*, vol. 48, pp. 25–33, 1995.

[12] O. Krauss. Design and Test of a lab-scale N20/HTPB Hybrid Rocket. *American Institute of Aeronautics and Astronautics*, 2003.

[13] Air Liquide. Nitrous Oxide Gas Data. *http://www.airliquide.com/en/business/products/gases/gasdata/index.asp?GasID=55*. Last accessed July 31, 2006.

[14] Aluminium City (Pty) Ltd. *Engineering Division Handbook*. Aluminium City (Pty) Ltd., 1999.

[15] R. A. Serway, R. J. Beichner, and J. W. Jewett. *Physics for Scientists and Engineers*. 6277 Sea Harbour drive, Orlando, FL 32887-6777, USA: Saunders College Publishing, fifth ed., 2000.

[16] Wikipaedia. Polypropylene Data. *http://en.wikipedia.org/wiki/Polypropylene*. Last accessed July 31, 2006.

[17] M. Hudson, A. Wright, C. Luchini, P. Wynne, and S. Rooke. Guanidinium Azo-Tetrazolate (GAT) as a High Performance Hybrid Rocket Fuel Additive. *Journal of Pyrotechnics*, vol. 19, pp. 37–42, 2004.

[18] M. Moran and H. Shapiro. *Fundamentals of Engineering Thermodynamics*. John Wiley and Sons, 3 ed., 1998.

III - Conclusion

The presented paper details the fundamental theory behind a hybrid rocket motor. It also presents the implemented design for the triggered-lightning study.

The total cost of ownership of this hybrid rocket is significantly less than other available rocket systems. This low total cost is reduced by the fact that the rocket is re-usable; allowing for a longer service life of components than other rockets. Practically this allows for more launches, and thus a larger and statistically more representative data set to be obtained.

Additionally the rocket does not contravene the South African explosive legislation, and is inherently safer than solid and liquid fuelled systems. The design allows for overpressures in both the oxidiser and combustion stages; and since triggering lightning cannot be viewed as a hazard free method having a large safety margin is vital in conducting a safe set of experiments.

The rocket is designed to survive direct attachment of the lightning mechanism. This is achieved by making the rocket body from aluminium, allowing the potential lightning current to flow on the external surface, without interfering with the combustion process.

The rocket has been constructed and tested. Several static tests were conducted, resulting in improved ignition and nozzle design. Full launches have also been done including the free flight of the rocket and testing of the launch rail. All systems function as expected.

Scope for further research

Improvements to the rocket might be possible, particularly in the ignition system. A butane-nitrous oxide flame could be substituted for the solid fuel block, but the problem of igniting that flame limits the implementation. Extra height could be achieved through aerodynamic improvements, however the rocket provides sufficient height to conduct the triggered-lightning study.

Now that the key component of the rocket triggered-lightning platform has been constructed, it is expected that research will progress in the following:

- Behaviour of electrical distribution systems with direct and induced lightning transients. Information generated through this research will enable power distribution companies to better understand the effects of the lightning phenomenon on the quality of power they provide; ultimately enabling industry to improve distribution networks and the quality of power supplied to electrical consumers.
- Behaviour of semi-conductor lightning protection elements. Research in this area will enable surge protection device (SPD) manufacturers to produce better products and afford consumers better lightning protection in the context of a more realistic system and provide a better understanding

of the behaviour of that system as a whole.

- Further research into the physical mechanism of the phenomenon thus providing researchers with a more accurate model of the lightning phenomenon, ultimately enabling further insights and predictions of the effects of lightning strikes.
- Confirmation of the attachment height to electric field magnitude relationships.
- Behaviour of the electromagnetic pulse from a lightning strike travelling over soil with a resistivity, unlike conditions found elsewhere where the resistivity is an order of magnitude smaller.

References

[1] B. Schonland. *The flight of thunderbolts*. Amen house, London, England: Oxford University Press, 1950.

[2] D. Pavanello, F. Rachidi, V. Rakov, C. Nucci, and J. Bermudez. *Return Stroke Current Profiles and Electromagnetic Fields Associated with Lightning Strikes to Tall Towers: Comparison of Engineering Models*. 27^{th} International Conference on Lightning Protection, 2004.

[3] V. Rakov and M. Uman. *Lightning: Physics and Effects*. The Edinburgh Building, Cambridge CB2 2RU, England: Cambridge University Press, 2003.

[4] V. Rakov, M. Uman, and K. Rambo. A review of ten years of triggered-lightning experiments at Camp Blanding, Florida. *Journal of Atmospheric Research*, vol. 76, pp. 503–517, 2005.

[5] K. Nonaka, T. Nakazawa, Y. Kinoshita, and H. Motoyama. *Measurement of Lightning Surge Characteristics of Footing Impedance on Actual 500kV Transmission Towers*. 27^{th} International Conference on Lightning Protection, 2004.

[6] Acts Online - South African Hypertext Legislation. Internet: http://www.acts.co.za, September 2005.

[7] M. D. Grant, J. Garrard, and K. J. Nixon. Low cost electric-field mill: Design, Construction and Testing. In *Proceedings of the 2006 Southern African Universities Power Engineering Conference*. Durban, South Africa, Jan. 2006.

[8] G. Sutton and O. Biblarz. *Rocket Propulsion Elements*. Wiley-Interscience, 7 ed., 2000.

[9] M. D. Grant and K. J. Nixon. Design of a re-usable rocket for triggered-lightning experiments - Paper 1363., Sep. 2006. Accepted for publication at the 28^{th} *International Conference on Lightning Protection* Kanazawa, Japan.

IV - Appendices

A Oxidiser stage design

This section presents a detailed discussion of the various parameters of the oxidiser (liquid) stage of a hybrid rocket motor. It forms the framework from which the behaviour of the liquid stage can be simulated.

A.1 Introduction

A hybrid rocket consists of a liquid oxidiser and a solid fuel stage. The oxidiser needs to be injected into the combustion chamber at a pressure higher than that in the combustion chamber or else back burn could occur into the oxidiser stage.

The use of an oxidising agent that is liquid at pressures lower than the expected operating pressure of the combustion chamber would require an additional pump to increase the pressure of the oxidiser stage in order to avoid back burn. This addition would greatly increase the weight of the rocket and is not a viable solution.

Gasses that are liquid at standard temperature under high pressures are ideal for this application; the most commonly available are liquid oxygen and nitrous oxide. The cryogenic property, or extremely low temperature of liquid oxygen under small sudden pressure drops, combined with the intense oxidising action of the gas yield it too dangerous to implement in this design.

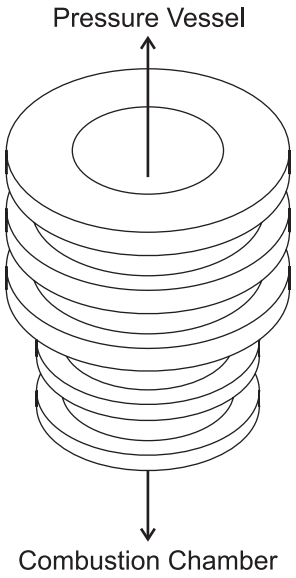

Figure A.1: Piston-Injector part which forms the bottom of the pressure vessel and injector into the combustion chamber

The liquid gas is housed in the top half of the rocket in a pressure vessel. As illustrated in *Figure A.1* this vessel is filled through a feed pipe, which is fed through the combustion chamber and terminates at the combustion chamber injector. The ignition phase burns through the feed pipe, effectively severing the connection, and allowing the pressurised gas to flow into the combustion chamber.

A.2 Nitrous Oxide

Nitrous Oxide, or Dinitrogen Oxide is described by the chemical formula N_2O. Depending on the charge on the oxygen atom, the bonds between the three atoms vary as shown in *Figure A.2*; however the bond to the oxygen atom is the weakest of the two bonds. This molecular structure is what makes N_2O such a potent oxidiser.

$$\boxed{N \equiv N^+ - O^- \longleftrightarrow N^- = N^+ = O}$$

Figure A.2: Molecular structure of nitrous oxide, showing weak and strong bonds

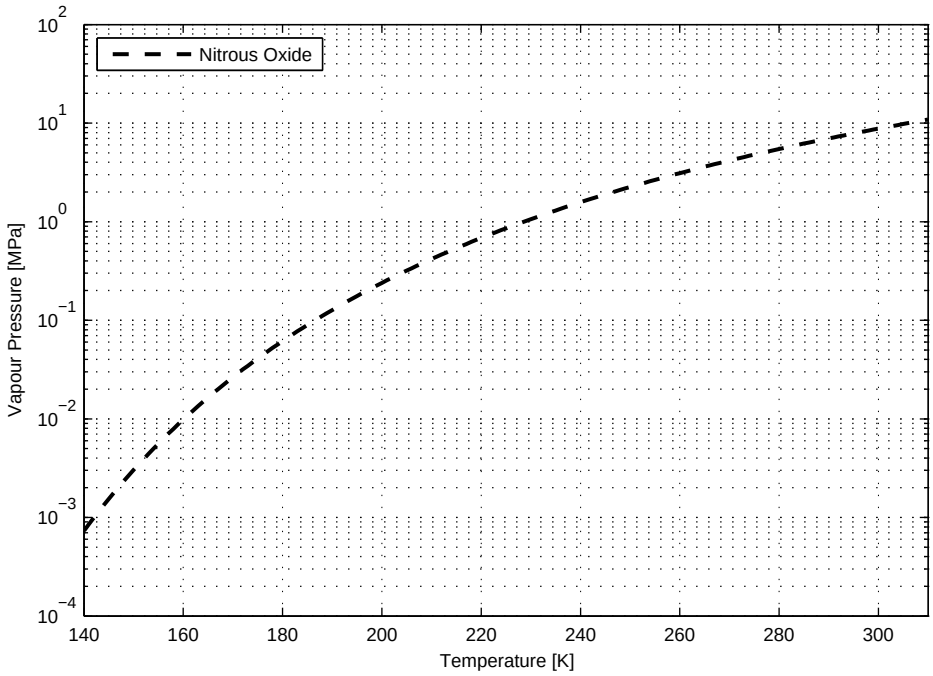

Figure A.3: Vapour pressure for nitrous oxide as a function of temperature as predicted by the Antoine equation

The Antoine equation approximates the vapour pressure for a pure substance with three dimensionless constants [1, 2]. The equation is given as:

$$\log_{10}(P) = A - \left(\frac{B}{T+C}\right) \tag{1}$$

Where:
P : Pressure [MPa]
T : Temperature [K]

Figure A.3 illustrates the prediction made by the Antoine equation for Nitrous Oxide from the constants given in *Table A.1* [3]. It exhibits the expected drop in pressure with temperature; a phenomenon expected whilst filling the rocket with the oxidiser as part of the launch preparation.

Table A.1: Antoine constants for nitrous oxide

Constant	**Value**
A	4.37799
B	621.077
C	-44.659

A.3 Pressure vessel

Taking the highest expected working vapour pressure as 6 MPa; an internal tube diameter of 34.9 mm, a tube wall thickness of 1.6 mm and a circlip grove depth of 0.75 mm: the following sections solve for the expected stresses.

A.3.1 Axial stress

Force exerted on the top cap due to the contained pressure is given by [4]:

$$\begin{aligned} F &= P \cdot A \\ &= 6 \times 10^6 \times \pi \left(\frac{34.9 \times 10^{-}3}{2}\right)^2 \\ &= 5.74 \text{ kN} \end{aligned} \tag{2}$$

Where:
F_p : Force [N]
P : Pressure [Pa]
A : Cross sectional area [m^2]

Hence the pressure exerted on the top-cap, see *Figure A.5*, by the gas contained within the tube translates to an axial stress on the pressure vessel, since the top-cap is attached to the end of the tub. This axial stress is given by [5]:

$$\begin{aligned} \sigma_a &= \frac{F}{A_a} \\ &= \frac{5.74 \times 10^3}{9.94 \times 10^{-}4} \\ &= 57.70 \text{ MPa} \end{aligned} \tag{3}$$

Where:
σ_a : Axial stress [Pa]
F : Force [N]
A_a : Cross sectional area [m^2]

Hence the cross sectional area of the tube, at the thinnest point, must be large enough to accommodate for the force exerted on it by the top-cap. Taking the mechanical properties of the tube from *Table 2*, there is a 300% safety margin.

A.3.2 Hoop stress

Now the contained pressure also exerts a force onto the inner surface of the pressure vessel, which is the tube wall of the rocket. This is realised as a tangential stress which is termed "Hoop stress" [5]. This stress acts as though it were to increase the diameter of the tubing and will cause longitudinal cracking and failure. Now because failure from containing a pressure will begin at the internal surface, the internal radius is used [5].

$$\begin{aligned} \sigma_h &= \frac{Pr}{w} \\ &= \frac{6 \times 10^6 \times 34.9 \times 10^{-3}}{1.6 \times 10^{-3}} \\ &= 130 \text{ MPa} \end{aligned} \tag{4}$$

Where:
σ_h : Stress [Pa]
P : Pressure inside vessel [Pa]
r : Outer radius of tube [m]
w : Thickness of tube [m]

As expected the thicker a piece of tubing, the more pressure it can withstand; however a larger diameter tube experiences an increased Hoop stress, as illustrated in *Figure A.4*. Still in the design, there is a safety margin of 2.5 MPa or 70%, a highly unlikely pressure given the expected vapour pressure predicted in *Figure A.3*.

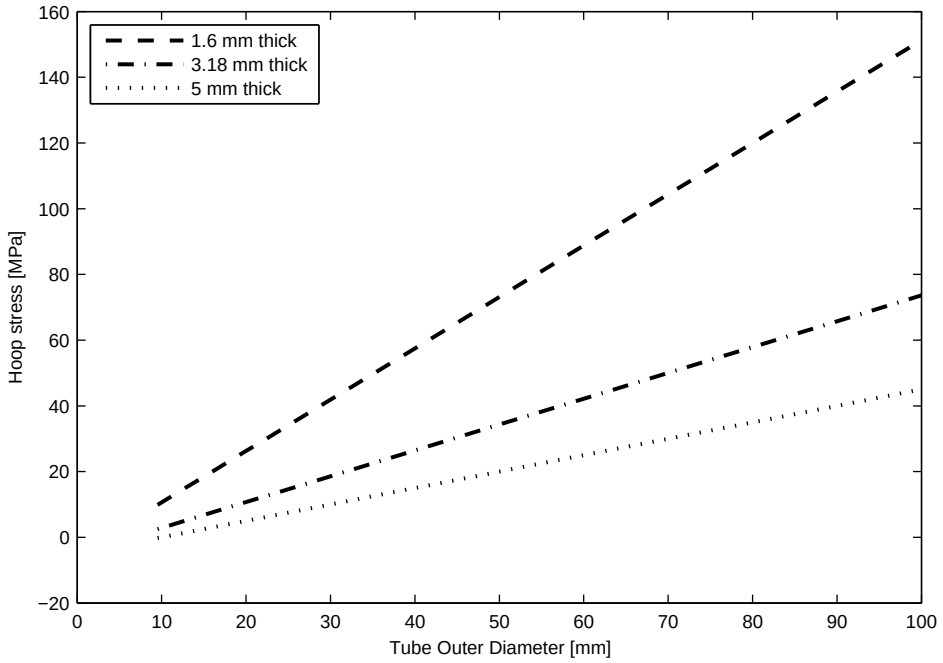

Figure A.4: A comparison of Hoop stresses for two thickness tubes and varying external diameters at a nominal internal pressure of 5 MPa

A.3.3 Seal design

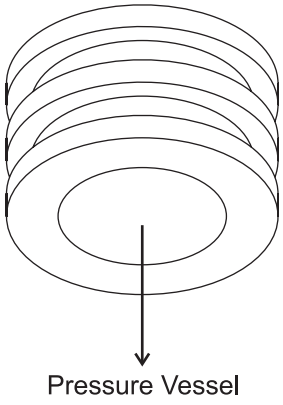

Figure A.5: Pressure vessel top cap with O-ring grooves

O-rings are manufactured to a number of standards, the metric standard ISO 3601 Part 1 defines groove width, depth and tolerance given the thickness of the O-ring chosen; the document also provides selection criteria of O-ring diameter for a required pressure seal [6].

O-rings deform under both pressure from the material seal as illustrated in *Figure A.6*, but also from the pressure differential across it as the O-ring seals.

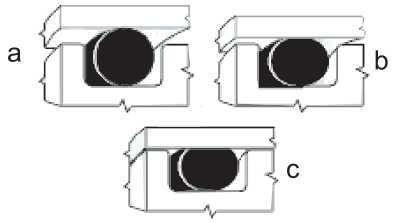

Figure A.6: O-ring gland: a) No deformation. b) Slight tangential pressure. c) Complete tangential pressure

As illustrated in *Figure A.5* and *Figure A.1*, the O-rings selected, and their grooves, have been designed to seal at a pressure greater than that the material can withstand, as predicted by *Equation 4* and specified in *Table 2*.

A.3.4 Combustion injection

The thrust of the rocket and rate of combustion is controlled by the mass flow rate of the oxidiser into the combustion chamber. This rate is a function of differential pressure between the oxidiser tank and combustion chamber [4], and the parameters of the piston/injector part, shown in *Figure A.1*.

$$\dot{m}_o = \frac{CA_t\sqrt{2\rho_o\Delta p}}{\sqrt{1-\gamma^2}} \tag{5}$$

Where:
$\dot{m}_o$: Mass flow rate [kg/s]
C : Discharge co-efficient
A_t : Injector cross-sectional area [m^2]
ρ_o : Fluid density [kg/m^3]
Δp : Differential pressure across nozzle [Pa]
γ : Area expansion ratio

The area expansion ratio, is determined from the nozzle throat diameter and combustion chamber cross-sectional area:

$$\gamma = \frac{A_t}{\pi \times R(t)^2} \tag{6}$$

Where:
γ : Area expansion ratio
A_t : Nozzle cross-sectional area [m^2]
$R(t)$: Combustion chamber radius [m]

A.4 Conclusion

Of the oxidiser stage design, the greatest concern lies in the pressure vessel and its ability to withstand both the high pressure and the low temperature under repeated stressing. The properties of the injector part and the tank pressure determine the rate at which combustion progresses and ultimately the thrust of the rocket.

The designed rocket is capable of withstanding the high pressure and low temperature of the oxidiser; these parameters are the most critical elements of the oxidiser stage. The flow of oxidiser ultimately regulates the rate of combustion in the combustion chamber, which affects the thrust produced by the combustion chamber and nozzle combination.

References

[1] M. Moran and H. Shapiro. *Fundamentals of Engineering Thermodynamics*. John Wiley and Sons, 3 ed., 1998.

[2] General Chemistry Online. FAQ: Liquids: What is the Antoine equation? *http://antoine.frostburg.edu/chem/senese/101/ liquids/faq/antoine-vapor-pressure.shtml*. Last accessed July 31, 2006.

[3] National Institute of Standards and Technology. NIST Chemistry WebBook. *http://webbook.nist.gov/chemistry/*. Last accessed July 31, 2006.

[4] R. A. Serway, R. J. Beichner, and J. W. Jewett. *Physics for Scientists and Engineers*. 6277 Sea Harbour drive, Orlando, FL 32887-6777, USA: Saunders College Publishing, fifth ed., 2000.

[5] K. Newman. *Tubing limits for burst and collapse*. CTES, L.C. 9870 Pozos lane, Conroe, Texas, 77303, USA, 2002.

[6] International Organisation for Standardization. *ISO 3601 Fluid power systems: O-rings, Part 1: Inside diameters, cross-sections, tolerances and size identification code*. International Organisation for Standardization, 1995.

B Combustion stage design

This section presents a detailed discussion of the various parameters of the combustion (solid) stage of the hybrid design. The section details how the behaviour of this stage depends on both the physical properties of the chamber and the flow of liquid oxidiser into it.

B.1 Introduction

Following the hybrid design methodology, the combustion chamber is both the source of fuel on which the oxidiser acts, and the place where combustion occurs. As a result there are the following restrictions on the design [1, 2, 3]:

1. Combustion is limited to a finite time.
2. Combustion chamber dimensions change with time.
3. Fuel production rate changes with time.

B.2 Structural considerations

The combustion stage therefore needs to be constructed from a material that will readily burn with assistance from the oxidiser. However the material will need to retain as much of its structural properties as possible during combustion as axial failure will result in movement of the injector part, see *Figure A.1.* The material also needs to insulate the heat generated in the chamber from the body of the rocket as temperature extremes will affect the temper, and hence strength, of the body material of the rocket. Thus not all of the material of the combustion chamber is burnt during a rocket fire, with the remnants providing the structural support and thermal insulation to the rocket.

Nitrous oxide will assist in the incineration of a variety of polymers, including polypropylene, polyethylene, hydroxyl-terminated polybutadiene (HTPB) and Polyvinyl chloride (PVC) [4]. Most can be designed to provide sufficient structural support to the injector part, and thermal insulation to the body. However of the four primary choices, polypropylene is the cheapest to obtain, and provides a sufficiently large source of energy to achieve efficient combustion [4]. Polypropylene is also easily machinable, with no special requirements needed to form the combustion chamber.

B.3 Regression behaviour

The combustion process of a hybrid rocket is illustrated in *Figure B.1* [2], and continues as long as fuel vapour is formed and oxidiser is injected.

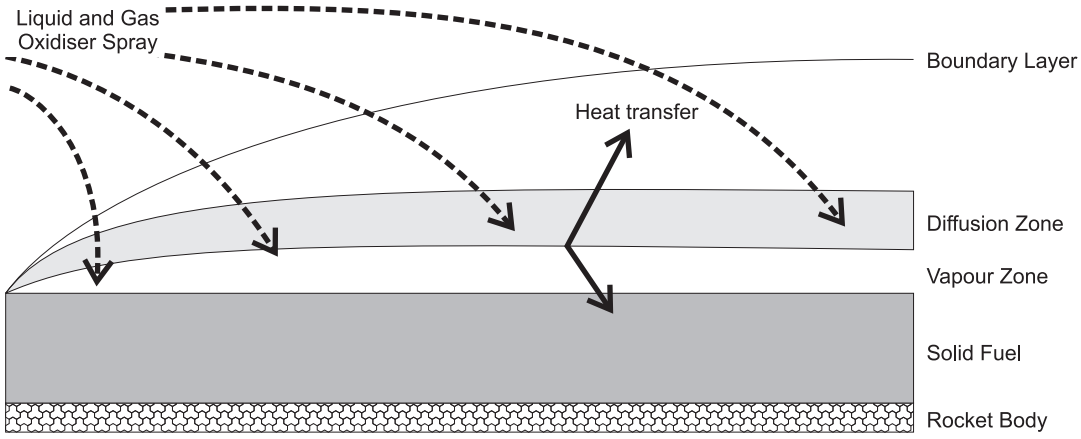

Figure B.1: Illustration of diffusion controlled combustion in hybrid rockets

Initially vapour is formed during the ignition phase of the rocket, where the heat from igniter burning degrades the surface of the solid stage. Rocket combustion then occurs once the oxidiser is injected into the combustion chamber mixing with the hot degraded solid fuel vapour which then burns further.

Combustion continues because heat from the combustion causes more solid fuel to degrade and vaporise. The heat is transferred by both convection and radiation to the surface of the solid fuel from the combustion zone boundary. This boundary is between the diffusion zone and vapour zone, as illustrated in *Figure B.1.* The combustion is limited to the confines of the oxidiser and vapour mix, illustrated by the boundary layer in *Figure B.1.*

The rate at which the fuel vapour is formed is given by [1, 2]:

$$\dot{m}_f = 2a\pi^{1-n}\rho_f L(m_o^n)R^{1-2n} \tag{1}$$

Where:
$\dot{m}_f$: Rate of fuel formation [kg/s].
a : Regression rate co-efficient
n : Regression rate exponent
ρ_f : Density of solid phase [kg/m^3]
L : Length of solid phase [m]
R : Radius of combustion chamber [m]

The regression rate constants are solid phase material specific, and can be construed as constants which describe the rate at which the polymer degrades under steady state combustion.

The mass flow rate of oxidiser into the combustion chamber is governed by the pressure differential between the vapour pressure in the oxidiser tank and in the combustion chamber. By designing the oxidiser injector to allow flow into the combustion chamber at the maximum expected combustion chamber pressure, optimum steady state combustion is ensured. However this injection profile has the risk that the

oxidiser will flood the chamber and remove too much heat, and halt vapour production. It is vital that the ignition phase heats the polymer up to a sufficient degree that sufficient polypropylene has degraded before the oxidiser is injected.

The chamber pressure is given as [2]:

$$p_1 = \frac{\dot{m} c^*}{g_0 A_t} \tag{2}$$

Where:

p_1 : Combustion chamber pressure [Pa]
$\dot{m}$: Mass flow rate ($\dot{m} = \dot{m}_f + \dot{m}_o$) [kg/s]
c^* : Chamber characteristic velocity [m/s]
g_0 : Gravity [m/s^2]
A_t : Nozzle throat area [m^2]

Now the rate of expansion of the radius of the combustion chamber, termed the regression rate is given as [1, 2]:

$$R(t) = \left(at(2n+1)(m_o/\pi)^n + R_i^{(2n+1)} \right)^{1/(2n+1)} \tag{3}$$

Where:

R : Radius of combustion chamber [m]
a : Regression rate co-efficient
t : Time from combustion start [s]
n : Regression rate exponent
R_i : Initial radius of combustion chamber [m]

From *Equation 3*, the amount of fuel expended in a burn can be predicted. However this requires accurate modelling of the oxidiser injection, and hence the design of the solid fuel stage must continue in a simulation study.

B.4 Conclusion

Central to the design of an efficient hybrid rocket is the combustion chamber; as it is both the source of fuel and provides structural support to the oxidiser pressure vessel. Although the behaviour of the combustion chamber is well understood, the dependence of its behaviour on the mass flow rate of the oxidiser into the chamber makes an analytical approach to designing various elements of this stage tedious and erroneous. Instead, the design was continued in the simulation study, *Appendix D*, where the geometry was calculated [1, 2].

This design uses polypropylene due to the fact that it is both cheap and easily obtainable as well as easily machineable into the parts required. Additionally the designed tube of the polymer is able to provide sufficient structural support at small wall thicknesses.

References

[1] O. Krauss. Design and Test of a lab-scale N20/HTPB Hybrid Rocket. *American Institute of Aeronautics and Astronautics*, 2003.

[2] G. Sutton and O. Biblarz. *Rocket Propulsion Elements*. Wiley-Interscience, 7 ed., 2000.

[3] M. Hudson, A. Wright, C. Luchini, P. Wynne, and S. Rooke. Guanidinium Azo-Tetrazolate (GAT) as a High Performance Hybrid Rocket Fuel Additive. *Journal of Pyrotechnics*, vol. 19, pp. 37–42, 2004.

[4] M. Wey and C. Chang. Kinetic study of polymer incineration. *Polymer Degradation and Stability*, vol. 48, pp. 25–33, 1995.

C Nozzle design

This section presents the design of the nozzle used on the hybrid rocket. It determines how the combustion chamber pressure and specific mass velocity of the combustion products are transformed into thrust. It completes the framework from which an accurate simulation study can be performed.

C.1 Introduction

The hot, rapidly expanding combustion products from the combination of the liquid oxidiser and degraded solid fuel in the hybrid rocket are expelled from the combustion chamber, since a pressure differential exists between the chamber and ambient. This expulsion is done through the nozzle, which ultimately determines the mass flow rate, given the pressure and density of the flow.

Supersonic nozzles typically consist of a convergent zone, a throat where flow is at Mach 1, and a divergent zone; the typically conical shape at the end of rockets.

C.2 Nozzle theory

In order to simplify the design process a number of assumptions about the flow and the constituents are made; Sutton states the following assumptions, and assigns a maximum 6% variance to them [1, pg 47]:

- Mass flow constituents are homogenous.
- Mass flow is gaseous, there are no solid or liquid constituents.
- The gas obeys the ideal gas law.
- Flow is adiabatic, and no energy is lost across mechanical elements.
- No friction or boundary layer effects.
- Flow is smooth, with no shock waves or discontinuities. Pressure, temperature and density are uniform through any section of the nozzle.
- Flow is axially directed to allow for a single dimension solution.
- Combustion is complete by the time the contents from the combustion chamber reach the nozzle.

Applying the principle of the conservation of mass across the nozzle, that is that mass flow rate throughout the nozzle is the same, and that the velocity of the flow depends on the cross sectional area:

$$\dot{m} = A_t/v \tag{1}$$

Where:
$\dot{m}$: Mass flow rate [kg/s]
A_t : Cross sectional area [m^2]
v : Flow velocity [m/s]

The specific heat ratios are defined for the perfect gas; and are related as follows [1, 2]:

$$k = c_p/c_v \tag{2}$$
$$c_p - c_v = \mathcal{R}/J \tag{3}$$
$$c_v = k\mathcal{R}/(k-1)J \tag{4}$$

Where:
k : Specific heat ratio
c_p : Specific heat at constant pressure [J/kg·K]
c_v : Specific heat at constant volume [J/kg·K]
$\mathcal{R}$: Gas constant per unit weight [J/kg·K]
J : Mechanical equivalent of heat, $J = 4.186$ [J/cal]

Now the speed of sound in the gas; and Mach number or ratio of flow velocity to the speed of sound, are defined as follows [2]:

$$v_s = \sqrt{k\mathcal{R}T} \tag{5}$$
$$M = v/v_s = v/\sqrt{k\mathcal{R}T} \tag{6}$$

Where:
v_s : Speed of sound [m/s]
v : Flow velocity of the gas [m/s]
T : Temperature of the gas [K]

An isentropic expansion is one where the entropy remains constant. Such an expansion occurs in the divergent zone of an ideal nozzle; and as expected the specific volume increases, but what is not expected is that the temperature does not drop as much. Now when the flow is stopped, stagnation conditions occur which are described by:

$$T_0 = T + v^2/(2c_pJ) \quad (7)$$

$$= T\left(1 + \frac{1}{2}(k-1)M^2\right) \quad (8)$$

Where:
T_0 : Stagnation temperature of gas [K]
T : Temperature of the gas [K]
v : Flow velocity of the gas [m/s]

The exhaust velocity of the gasses out of a nozzle for a given inflow velocity is [1, 3]:

$$v_e = \sqrt{\frac{2k}{k-1}\mathcal{R}T\left[1 - \left(\frac{p_e}{p_c}\right)^{(k-1)/k}\right] + v_c^2} \quad (9)$$

Where:
v_e : Exhaust velocity [m/s]
k : Specific heat ratio
$\mathcal{R}$: Gas constant per unit weight [J/kg·K]
T : Absolute temperature of the gas [K]
p_e : Exhaust pressure [Pa]
p_c : Chamber pressure [Pa]
v_c : Inflow velocity [m/s]

Hence the exhaust velocity depends on the pressure ratio between the inlet and exit of the nozzle; the specific heat ratio of the gas and the combustion temperature or thermal energy of the gas.

The critical pressure in the nozzle is found when the mass flow rate is at a maximum; *Equation 1* predicts that this will occur at the throat of the nozzle, where the cross sectional area is the smallest. Incidentally the Mach number is 1 at this point [2].

$$\epsilon = A_e/A_t \quad (10)$$

$$p_t/p_c = (2/(k+1))^{k/(k-1)} \quad (11)$$

Where:
ϵ : Area expansion ratio
A_e : Nozzle exit cross sectional area [m^2]
A_t : Nozzle throat cross sectional area [m^2]
k : Specific heat ratio
p_t : Thoat pressure [Pa]
p_c : Chamber pressure [Pa]

The mass flow rate can be expressed in terms of the throat area of the nozzle and the chamber pressure:

$$\dot{m} = \frac{A_t v_c}{V_t} = A_t p_c k \frac{\sqrt{(2/(k+1))^{(k+1)/(k-1)}}}{\sqrt{kRT}} \tag{12}$$

Where:
A_t : Nozzle throat cross sectional area [m^2]
v_c : Inflow velocity [m/s]
V_t : Nozzle throat volume [m^3]
p_c : Chamber pressure [Pa]

The change in thrust during the flight of the rocket through 1000 m due to variance in atmospheric pressure is less than 2% [1, pg 68], and this term is removed for simplification. Finally the thrust can be determined from [1]:

$$F = \dot{m} v_e + (p_n - p_e) A_n \tag{13}$$

Where:
F : Force [N]
$\dot{m}$: Mass flow of material [kg/s]
p_n : Nozzle throat pressure [Pa]
p_e : Exhaust gas pressure [Pa]
A_n : Nozzle cross-sectional area [m^2]

C.3 Nozzle design

As the nozzle ultimately converts thermal energy of the combustion products into kinetic energy through the supersonic expansion of the gasses; the reverse process can be seen to occur at points where the flow velocity is hampered. Essentially kinetic energy is converted into thermal energy at these points, termed stagnation points, and the temperature increases dramatically. The combined energy, converted to thermal energy can exceed 3 000 K. With this in mind, the throat, or the section of the nozzle with the smallest cross sectional area must be free from any blemishes as rapid and severe erosion will occur.

The nozzle is constructed from high density carbon due to the excellent thermal tolerances of the material, and that fact that it is easy to machine. *Figure C.1* presents the detailed design of the nozzle, clearly illustrating the convergent, throat and divergent sections. The nozzle also includes a small groove in which an O-ring is seated, in order to seal the chamber and prevent the leak of any hot gases onto the body of the rocket.

Since the fuel is only expected to be used once; the O-ring is only expected to survive a single flight. Hence a standard rubber O-ring is used, and during the burn it will melt and probably bond to the surface of the plastic. This is not a concern since O-rings are cheap and thermal protection of the O-ring will increase the cost of the rocket above that of replacing the O-ring.

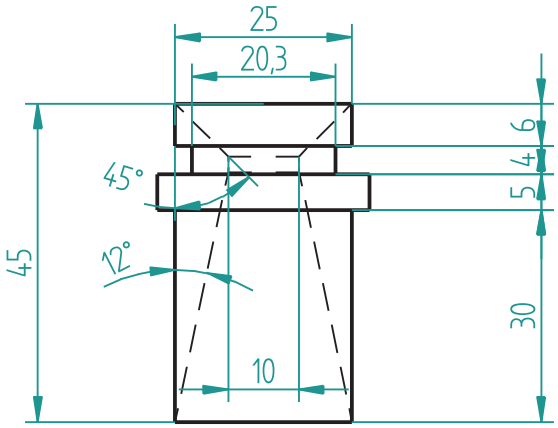

Figure C.1: Nozzle design, illustrating convergent, throat and expansion sections

Similar to the combustion chamber design, the parameters of the nozzle are determined from the simulation model, as the thrust behaviour depends on the behaviour of the combustion and oxidiser stages.

Since a nozzle cannot completely expand the gasses to atmospheric pressure, the gas within the immediate exhaust plume expands and contracts as it attempts to both slow down and reach ambient pressure. These contractions, called Mach diamonds, are visible in correctly designed nozzles as the exhaust flow has to be supersonic for the boundary conditions to produce the contractions [1, 3]. These Mach diamonds have been sighted in the rocket's static and flight tests.

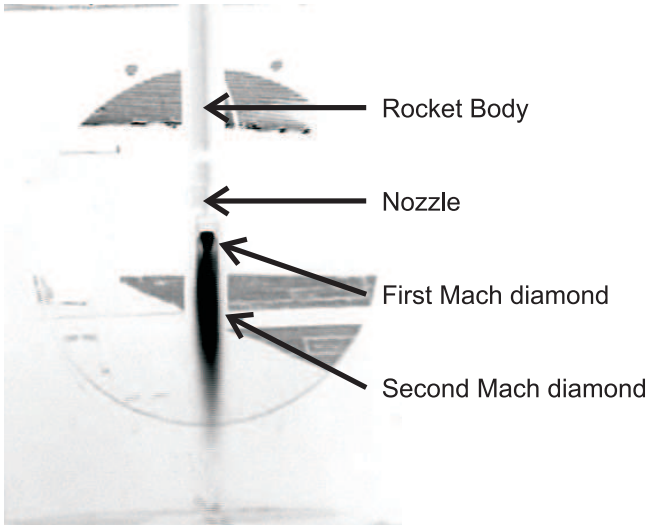

Figure C.2: Inverted image of static test of designed rocket, showing Mach diamonds

C.4 Conclusion

This appendix has presented the underlying nozzle theory which has been implemented in the model. From the simulation study, the parameters of the nozzle were determined. The material from which the nozzle was constructed was selected for its thermal withstand properties as the stagnation temperatures are of a great concern.

The next section to be presented is that of the simulation study which effectively ties the previous three appendices together.

References

[1] G. Sutton and O. Biblarz. *Rocket Propulsion Elements*. Wiley-Interscience, 7 ed., 2000.

[2] M. Moran and H. Shapiro. *Fundamentals of Engineering Thermodynamics*. John Wiley and Sons, 3 ed., 1998.

[3] O. Krauss. Design and Test of a lab-scale N20/HTPB Hybrid Rocket. *American Institute of Aeronautics and Astronautics*, 2003.

D Simulation Model

The simulation model from which the behaviour of the rocket motor was predicted is presented in this section. It uses the framework provided by the appendices that describe the oxidiser, combustion and nozzle stages; and ultimately predicts the apogee of the rocket's flight.

D.1 Introduction

The previous three sections have presented, in order, the behaviour and designs of: the oxidiser stage, the combustion stage and the nozzle. Due to the increasing dependence of each stage on the behaviour of the previous stage, the only suitable design pattern to follow was that of a simulation study. The resulting simulated rocket can tow a section of thin copper wire to a height of 1 km above the launch height.

D.2 General Model

As illustrated in *Figure D.1*, the model was divided into three primary elements: the liquid gas tank, called "NOS Tank"; the combustion chamber which responds to the mass flow into it; and the flight system which responds to the thrust produced by the combustion chamber.

However there are some feedback loops between the various elements:

1. Combustion chamber pressure affects pressure differential across nozzle that injects liquid gas into the chamber. As a result, as combustion progresses, and chamber pressure increases, mass flow of oxidiser is reduced.
2. The combustion chamber radius expands with combustion as described by the regression equations presented previously. This affects the expansion of the liquid gas, and hence the mass flow through the injector.
3. The weight of the rocket decreases as mass is expelled to create thrust, but the weight of the wire attached to the rocket increases as the rocket flies upwards. Hence there is a mass model which ties all three sub-systems together.

The inertial effects of the masses within the rocket have been accounted for; as has the reduction in mass of the oxidiser as combustion progresses. Hence the flight system needs to be aware of the mass of the rocket, which is generally determined by the mass of oxidiser still present and the weight of the body; the former varying with time.

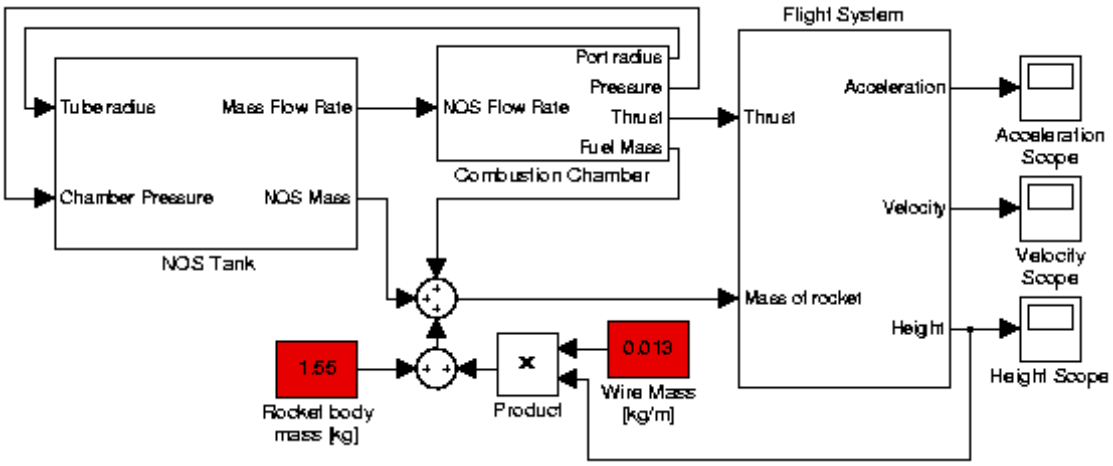

Figure D.1: Rocket simulation model schematic

D.3 NOS tank subsystem

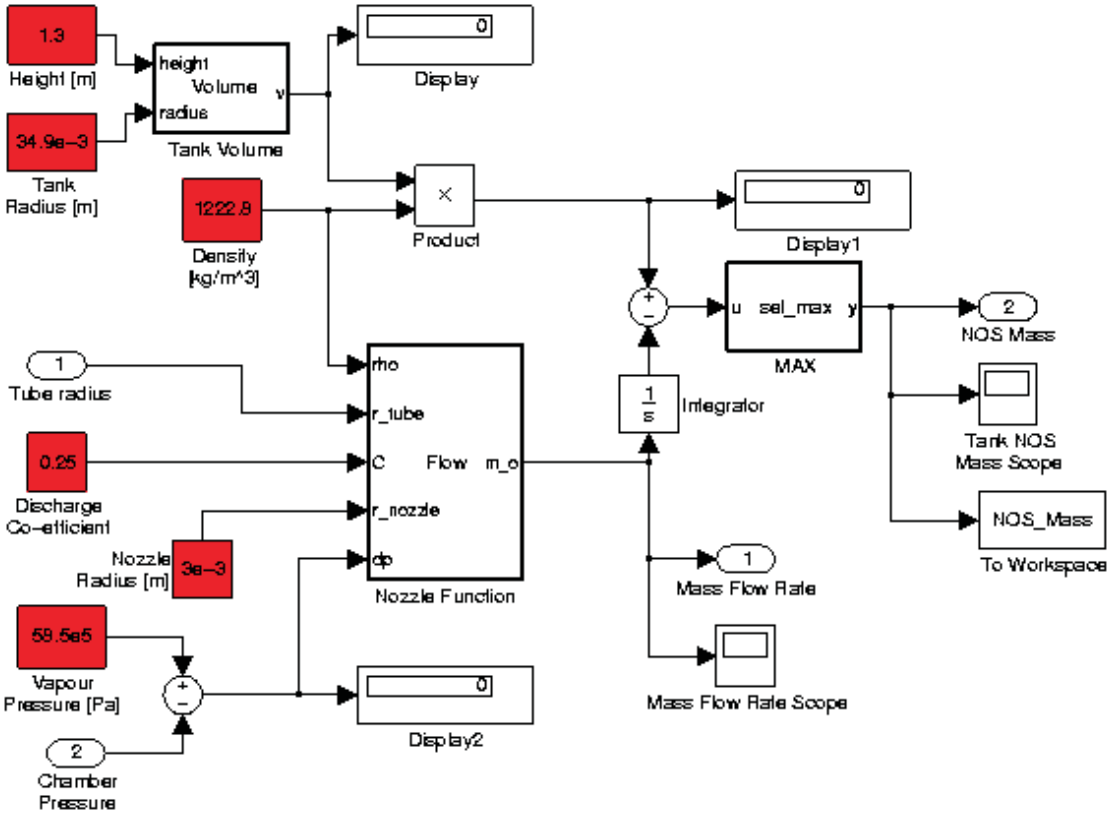

Figure D.2: NOS tank model schematic

Table D.1: NOS tank constants

Name	Value	Units
Density	1222.8	kg/m^3
Discharge co-efficient	0.25	–
Height	1.3	m
Nozzle Radius	3e-3	m
Tank Radius	34.9e-3	m
Vapour Pressure	58.5e5	Pa

The tank is filled with liquid nitrous oxide, which is assumed to be at constant temperature, and hence constant density. This simplification allows the removal of a subsystem that would calculate vapour pressure given the temperature of the liquid, see *Section A.2*. This simplification greatly increases simulation speed and the approximation has little effect on the design parameters.

Hence the volume of liquid N_2O in the tank is easily calculated and is implemented in the "Tank volume" block shown in *Figure D.2*, which contains the code below:

Tank Volume Code

```
function v = Volume(height, radius)
% This block supports an embeddable subset of the MATLAB language.
% See the help menu for details.

v = pi * (radius^2) * height;
```

End of Code

The oxidiser mass flow rate as explained in *Equation 5* in *Section A.3.4* is implemented in the "Nozzle function" block, illustrated in *Figure D.2*, with oxidiser chamber pressure, combustion chamber pressure and injector parameters ultimately determining the mass flow rate. The code in this block is shown blow:

Nozzle function Code

```
function m_o = Flow(rho, r_tube, C, r_nozzle, dp)
% This block supports an embeddable subset of the MATLAB language.
% See the help menu for details.
m_o =max(0, C * (pi * r_nozzle^2) * sqrt(2*rho*dp) /  sqrt(1 - (r_nozzle /r_tube)^4));
```

End of Code

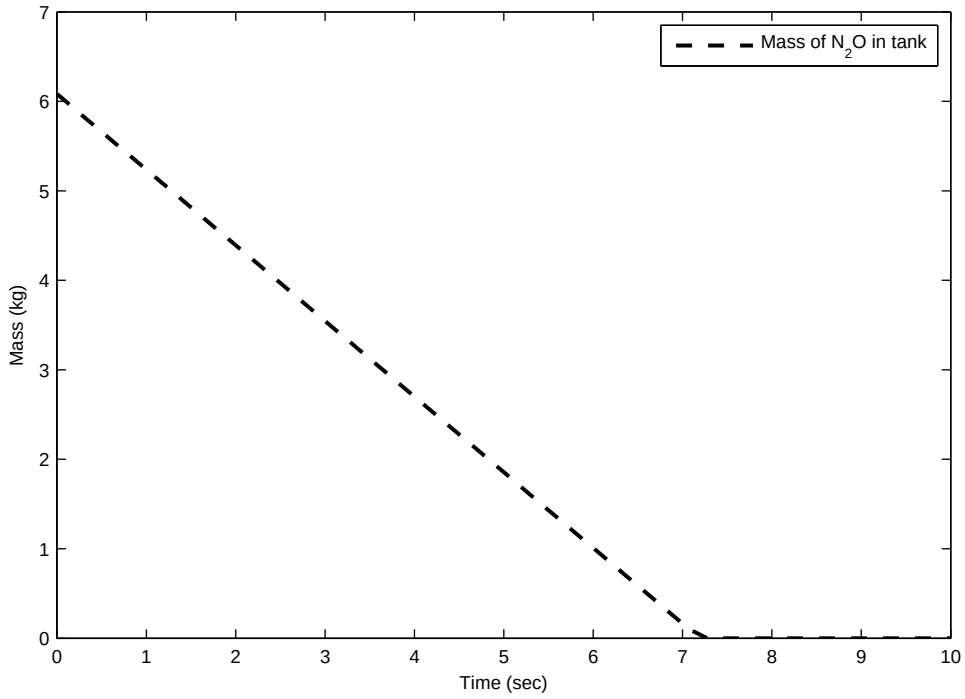

Figure D.3: Simulated mass of nitrous oxide over time

Table D.2: Combustion chamber constants

Name	**Value**	**Units**
Fuel Density	0.9	kg/m^3
Grain length	0.4	m
Grain Inner Radius	25e-3	m
Grain Outer Radius	34.9e-3	m
Loop Breaker	0	–
Regression Exponent	0.65	–
Regression Rate Co-efficient	9e-6	–
Specific Impulse	12	Ns

D.4 Combustion chamber subsection

The regression of the fuel grain, or the expansion of the combustion chamber, as fuel is produced is described by *Equation 3* in *Section B.3*. The behaviour depends on the initial conditions of the chamber: density, radius, fuel regression constants; and the mass flow rate of the oxidiser into the chamber. This function is implemented in the "Fuel Grain Regression" code block.

Fuel Grain Regression Code

```
function R = Port_R(m_o, a, n, t, R_i)
% This block supports an embeddable subset of the MATLAB language.
% See the help menu for details.
R = (a * t * (2*n + 1) * (m_o/pi)^n + R_i^(2*n + 1))^(1/(2*n + 1));
```

End of Code

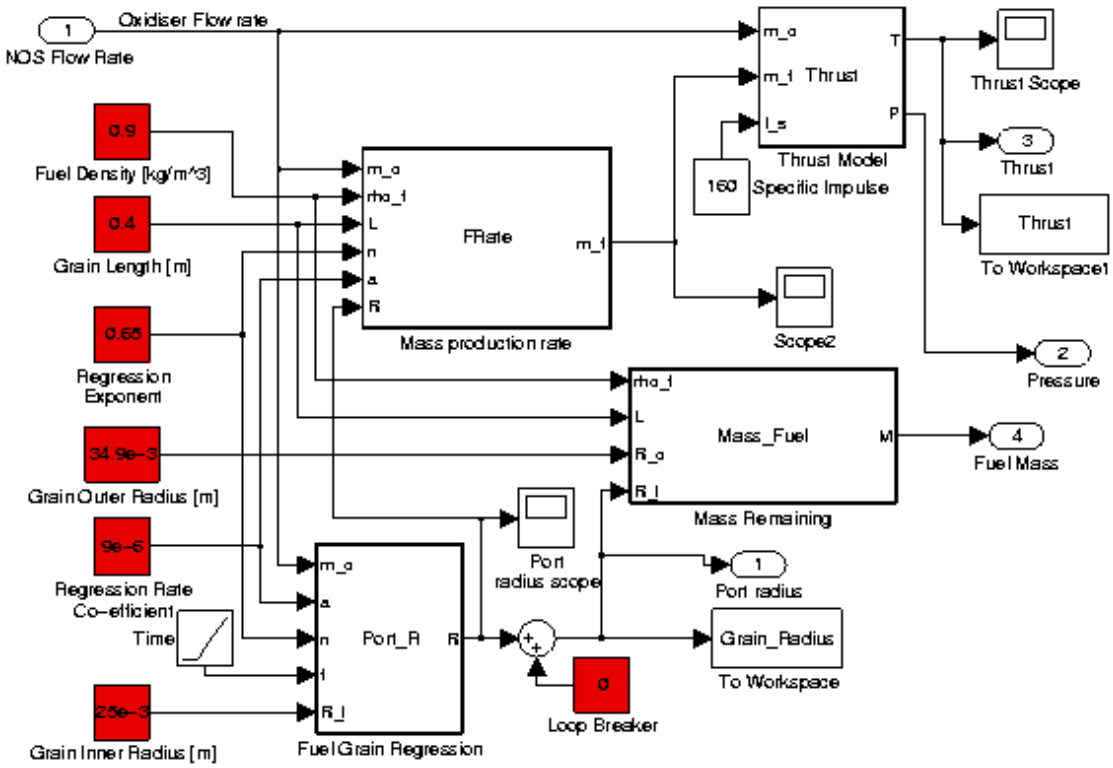

Figure D.4: Combustion chamber model schematic

The fuel production rate, or the rate at which vaporised solid fuel is formed from the heat of combustion depends on the surface area of the combustion chamber, the mass flow rate of oxidiser, and the regression constants of the solid fuel. This function described by *Equation 1* in *Section B.3* is implemented in the block titled "Mass production rate" which contains the code shown below:

Mass Production Code

```
function m_f = FRate(m_o, rho_f, L, n, a, R)
% This block supports an embeddable subset of the MATLAB language.
% See the help menu for details.
m_f = 2 * pi ^(1-n) * rho_f * L * a * (m_o^n) * R^(1 - 2*n);
```

End of Code

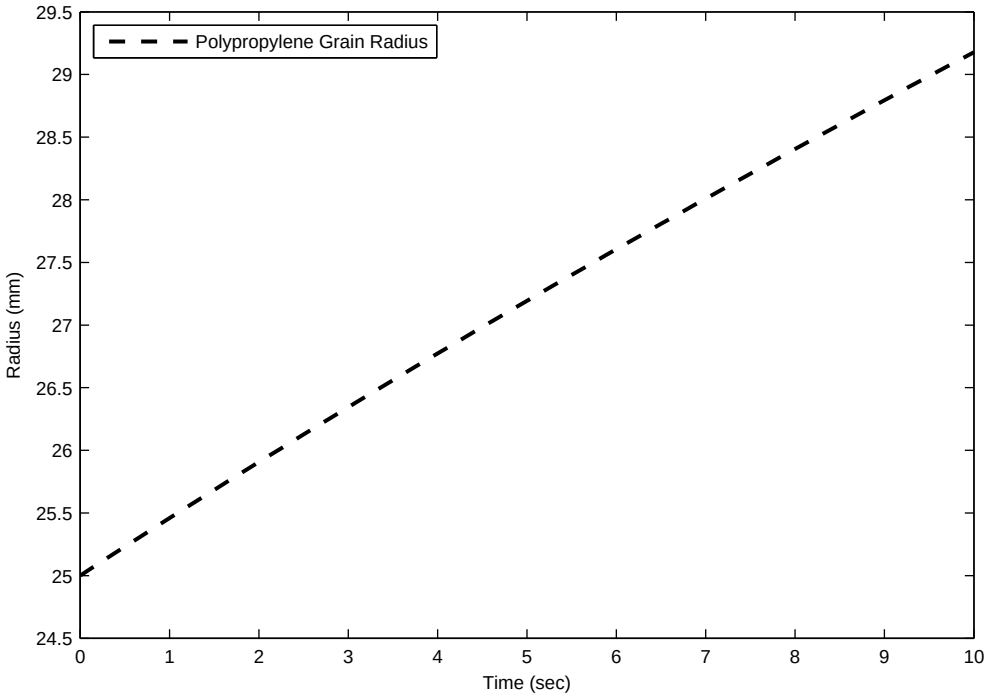

Figure D.5: Simulated regression of combustion chamber radius

In order to account for the effects of gravity against the rocket, the remaining mass of the solid fuel needs to be fed into the flight sub-system of the model. The mass is found by the volume - density product of the remaining fuel, shown in the equation below and implemented in the block titled "Mass remaining":

$$M = \pi \rho_f L (R_o^2 - R_i^2) \tag{1}$$

Where:

M : Mass of solid fuel remaining [kg].

ρ_f : Density of the fuel [kg/m^3

L : Length of solid fuel [m]

R_o : Outer radius of fuel [m]

R_i : Radius of combustion chamber [m]

Mass Remaining Code

```
function M = Mass_Fuel(rho_f, L, R_o, R_i)
% This block supports an embeddable subset of the MATLAB language.
% See the help menu for details.
M = L* rho_f * pi*(R_o^2 - R_i^2);
```

End of Code

The thrust of the rocket is given by *Equation 13* and a simplified version, which replaces the expansion ratio for that of a constant specific impulse is implemented in the block titled "Thrust" which contains the code below [1, 2]:

Thrust Model Code

```
function T = Thrust(m_o, m_f, I_s)
% This block supports an embeddable subset of the MATLAB language.
% See the help menu for details.
T = (m_o + m_f) * I_s * 9.8;
```

End of Code

D.5 Flight system subsection

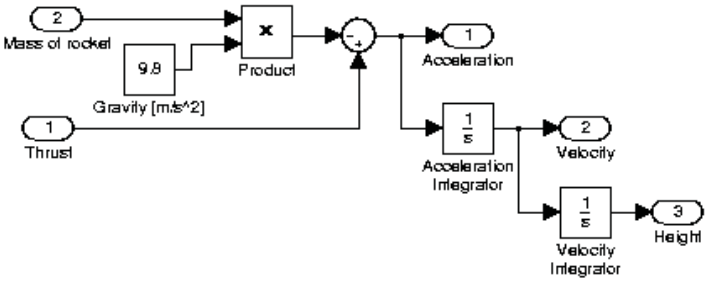

Figure D.6: Flight system model schematic

Table D.3: Flight system constants

Name	Value	Units
Gravity	9.8	m/s^2

This subsection calculates the acceleration of the rocket given the thrust produced by the rocket motor and the effects of gravity on the remaining mass of the rocket. The mass of the rocket includes the reduction from the fuel expelled to create thrust as well as the additional mass from the wire towed upwards by the rocket.

The subsystem system, shown in *Figure D.6*, used to calculate the velocity and height relies on classical mechanics as described in [3]. They are summarised below:

$$v = \int_0^t a(t) \cdot dt \tag{2}$$

$$h = \int_0^t h(t) \cdot dt \tag{3}$$

$$= \int_0^t \int_0^t a(t) \cdot dt^2 \tag{4}$$

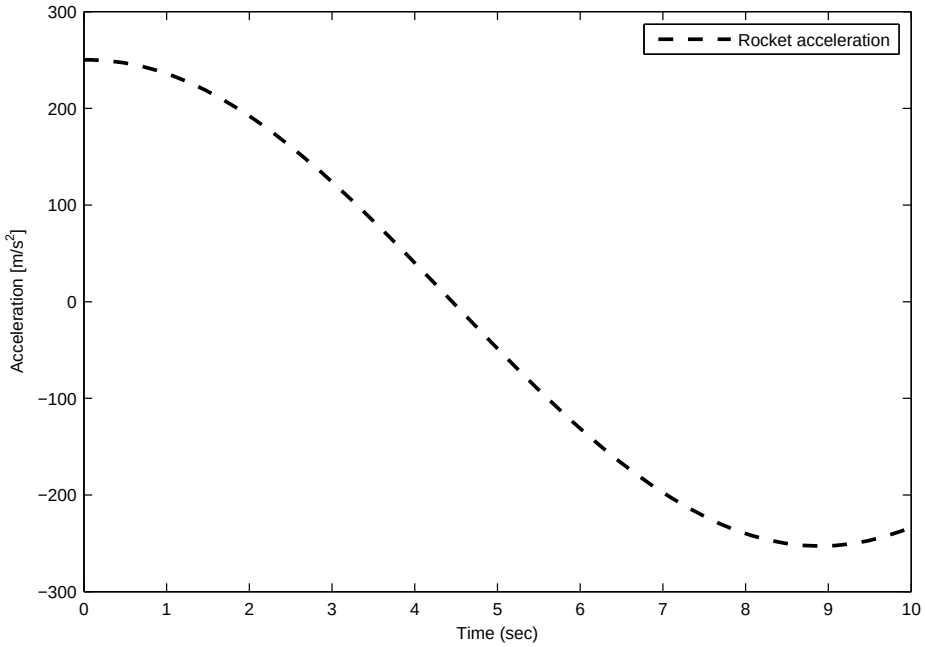

Figure D.7: Simulated acceleration of the rocket over time

At 5 seconds the weight of the wire attached to the rocket is equal to the thrust produced by the rocket and hence there is no acceleration. The rocket will continue to fly until the velocity reaches zero; this point is known as the apogee of the rocket's flight and the rocket starts falling to the ground.

Since velocity is the integral of the acceleration of the rocket, the peak velocity corresponds to the zero crossing point of the acceleration. The maximum speed is close on Mach 3, however this model ignores aerodynamic factors such as drag and hence the implemented maximum speed will be less.

Since the height is the double integral of the acceleration of the rocket, then the acceleration is the derivative of the velocity which in turn is the derivative of the distance above the ground with respect to time. So since the acceleration is negative at times after 5 seconds of flight, the height will continue to increase until the velocity becomes negative.

The rocket only really burns while liquid nitrous oxide is injected into the combustion chamber, the simulation predicts that this will end at around 7 seconds. However the simulation continues until ten seconds. The reason for continuing the simulation past the time that combustion ends is because the rocket will continue to gain height as the velocity decreases. The rocket will reach its apogee when the velocity is zero, and descends once the velocity becomes negative.

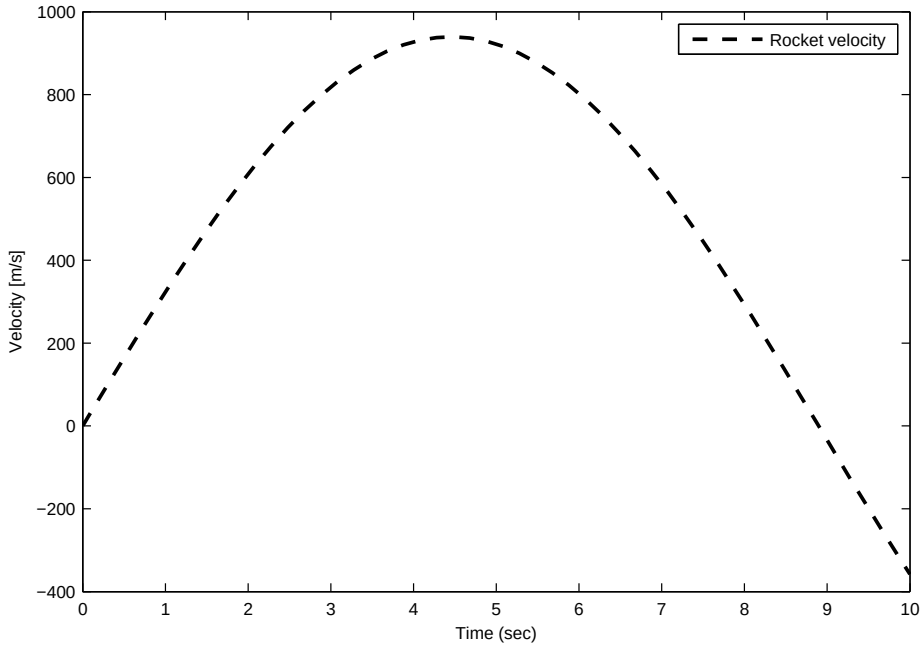

Figure D.8: Simulated velocity of the rocket over time

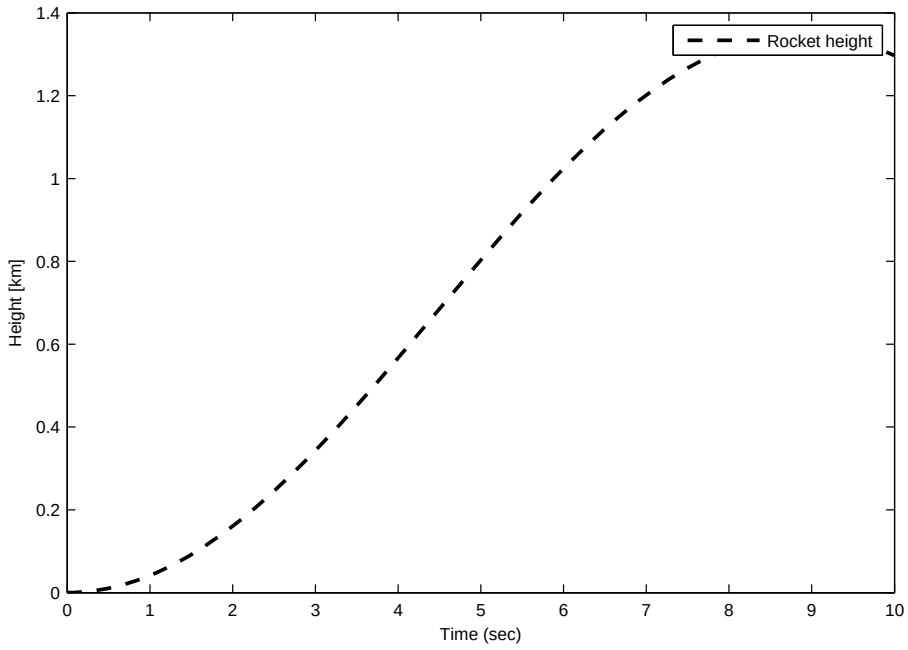

Figure D.9: Simulated height of the rocket over time

D.6 Conclusion

The simulation model presented is used to predict the behaviour of the rocket: expected acceleration, velocity and apogee. The model was integral in determining the parameters of the combustion and nozzles stages as their behaviour is dependent on that of the upstream stages. Particularly knowledge about the amount of plastic removed from the combustion chamber as the combustion regresses is vital in designing a combustion stage that can support the force from the pressurised upstream oxidiser stage.

Acceleration of the rocket is reduced by the increasing weight of the wire towed behind it. This addition alone makes a straight forward analytical approach to predicating the apogee of the rocket impossible. Instead the numerical approach, where the remaining mass of the rocket combined with that of the wire with the effects of gravity against the thrust produced yields a simple graph, *Figure D.9*, from which the behaviour is easily interpreted.

References

[1] G. Sutton and O. Biblarz. *Rocket Propulsion Elements*. Wiley-Interscience, 7 ed., 2000.

[2] O. Krauss. Design and Test of a lab-scale N20/HTPB Hybrid Rocket. *American Institute of Aeronautics and Astronautics*, 2003.

[3] R. A. Serway, R. J. Beichner, and J. W. Jewett. *Physics for Scientists and Engineers*. 6277 Sea Harbour drive, Orlando, FL 32887-6777, USA: Saunders College Publishing, fifth ed., 2000.

E Launch system

The mechanical design of the launch rail and interface onto the rocket is presented in this section. As the rocket has no active guidance, it needs to accelerate sufficiently before leaving the launch rail so that the static fins have enough influence to ensure straight flight. The tower that supports the launch rail and gas bottle is also presented.

E.1 Introduction

As the rocket only has passive fins, some form of guidance must be provided until the aerodynamic forces of the air flowing over the surface of the passive fins is sufficient to ensure stable flight. Given the acceleration of the rocket, it is expected that sufficient velocity will be achieved after 2 m of acceleration.

Taking the suggested the launch criteria for rocket triggered-lightning based on the incident electric field at ground level at 4 kV/m [1]; it is important to protect any researchers in the area, from the possible lightning currents, in a sufficiently protected structure. This precludes the researcher from any direct action associated with launching or re-loading a rocket on the launcher. Thus remote control commands must be sent to the launch system via a galvanically isolated link.

However, while the lightning attachment probability to the rocket for the electric field criteria of 4 kV/m is 95%, it is still possible that lightning will not attach to the launched rocket. Hence a few rockets need to be available to launch into the lighting storm. Thus the rocket launcher has been designed to hold four rockets, associated launch rails, fuel filling equipment and controllers.

E.2 Tower Design

The tower illustrated in *Figure E.1* shows the structural design of the tower. It is constructed such that a full bottle of N_2O can be suspended, inverted, within the frame. Hence the frame needs to be able to support the following:

1. Full, inverted bottle of N_2O.
2. Four fully loaded rockets.
3. Gas flow control solenoids.
4. Ignition system.
5. Power source (lead acid battery).
6. Launch rails for each rocket.

This means that the total weight onto the tower will be approximately 250 kg. The tower ideally should be erected and operated by a single person, and so the weight of the structure must be at an absolute minimum. For this purpose, the tower was constructed from high grade aluminium tubes. These tubes were then welded together to form the braces which provide the structural support. This is illustrated in *Figure E.1*.

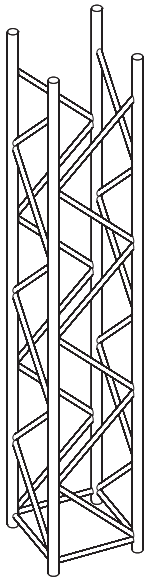

Figure E.1: Launch tower

Each corner of the tower supports a single launch rail. The launch rails are made from modified curtain rails, and the rocket is attached to the rails by means of curtain runners that are bonded to the surface of the body with epoxy resin.

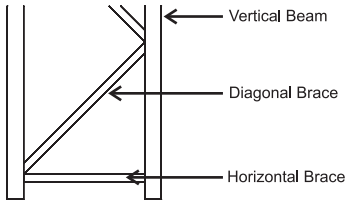

Figure E.2: Launch tower structural braces

A base, to prevent the tower from toppling over has also been constructed. The tower sits on top of the base, interfacing with four pins which are welded to the horizontal base.

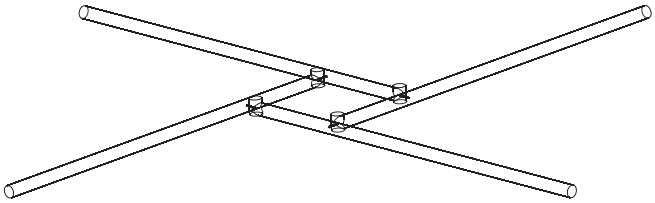

Figure E.3: Launch tower base, with interface pins

E.3 Control system

The pre-launch priming of the rocket consists of filling it with liquid nitrous oxide and is controlled with a gas solenoid. To open the solenoid, current needs to be fed through the solenoid coil. This current is controlled with a power MOSFET which takes the signal from a controlling microprocessor, and opens the feed. The solenoid is held open until liquid is detected at the vent jet; which indicates that the oxidiser stage is full.

Ignition of the rocket is controlled in a similar fashion. The rocket is filled until the liquid is detected, and then while keeping the solenoid open, current is driven into the ignition circuit. This circuit consists of a strip of resistive wire which heats up as the current flows through it. This heat is sufficient to initiate combustion on the surface of the solid fuel igniter. At this stage the rocket is now out of the control of the researcher.

Combustion progresses through the solid fuel block until is severs the liquid oxidiser feed pipe; at this point liquid oxidiser is injected into the combustion chamber and the rocket motor fire at full capacity and flies off the launch rail.

However, if the solid fuel block burns through the feed pipe before the surface of the combustion chamber is sufficiently degraded then the oxidiser, which rapidly cools due to adiabatic expansion, extinguishes the combustion process and the rocket will fail to launch. The remaining liquid oxidiser will then vent out of the rocket, through the combustion chamber and into the atmosphere. This condition, while visually obvious, is almost impossible to detect without the addition of another sensor. Since the rocket returns to an inert state regardless of wether combustion has occurred or not; it is assumed that if the ignition has been initiated that the rocket no longer contains compressed gas and is safe to approach.

Lightning protection of the tower is achieved through the protection of each solenoid with a metal oxide varistor (MOV) which will prevent any damage from lightning impulses. The tower itself is earthed and has a earth rod through which to dissipate the lightning current. This rod is driven into the ground before the tower base is placed, and can be removed once the experiment has been completed.

E.4 Conclusion

The final element of the triggered-lightning system has been presented, and since the launcher is responsible for the guidance of the rocket until the fins are sufficiently active the launcher is integral for the successful launch of a rocket.

The capability to launch more than one rocket has been provided, and each corner of the tower supports a rocket, launch rail and ignition system. The tower is isolated from the control system by means of a fibre optic data link through which remote control commands to fill and ignite each rocket are sent.

References

[1] V. Rakov and M. Uman. *Lightning: Physics and Effects*. The Edinburgh Building, Cambridge CB2 2RU, England: Cambridge University Press, 2003.

F Project expenditure

The project bill of materials and prototyping costs are presented for reference.

Table F.1 details the cost of the project. It includes all the materials acquired, and their cost. It also includes labour costs where items required construction at industrial facilities outside the School of Electrical and Information Engineering.

Table F.1: Table of expenses, including materials and labour

Item	**Quantity**	**Cost per Unit**	**Total**
Stainless	1	R 41.36	R 41.36
Al Rod (50d)	1	R 29.87	R 29.87
Al Tube	1	R 95.69	R 95.69
Liner	1	R 0.00	R 0.00
Machining	1	R 1024	R 1024
NOS (32kg)	1	R 598.35	R 598.35
Bottle rental	6	R 21.318	R 127.908
Plastic rod (Poly)	0.47	R 136.54	R 64.03
NOS Solenoid	1	R 550.00	R 550.00
Carbon Nozzle	1	R 250.00	R 250.00
Bull nose adapter	1	R 109.95	R 109.95
Gas fittings	1	R 429.47	R 429.47
Pressure Gauge	1	R 420.17	R 420.17
Gas fittings	1	R 167.47	R 167.47
Plastic rod (Poly)	1	R 136.54	R 136.54
Al Rod (50d)	1	R 8.00	R 8.00
Chemicals	1	R 63.00	R 63.00
MERC Chemicals	1	R 80.00	R 80.00
Al Rod (25d)	0.04	R 61.56	R 2.46
Al Rod (45d)	0.08	R 183.54	R 14.68
Al Rod (65d)	0.15	R 381.9	R 57.285
Plastic rod (Poly)	0.5	R 122.9	R 61.45
Al Tube (38.1d)	1.73	R 33.23	R 57.48
O-Rings	10	R 2.00	R 20.00
Plastic rod (Poly)	1	R 87.00	R 87.00
Circlips	10	R 2.85	R 28.50
Gas fittings	1	R 109.00	R 109.00
		Total:	R 4,524.68

G Technical Drawings

A complete set of technical drawings from which the rocket can be constructed are presented in this appendix. Materials, dimensions and tolerances are as indicated.

G.1 Drawings

The following sheets detail the technical drawings from which the rocket is constructed and assembled. The various parameters of the parts were determined from the simulation study.

Table G.1: List of technical drawing sheets for hybrid rocket construction and assembly

Sheet 1	Assembly diagrams with detail views of parts in placed positions.
Sheet 2	Rocket body part, with detail views of circlip grooves.
Sheet 3	Thermal insulator part
Sheet 4	Nozzle part
Sheet 5	Fuel grain part
Sheet 6	Piston/Injector Part
Sheet 7	Tank top part
Sheet 8	Fins part
Sheet 9	Tower Scaffolding
Sheet 10	Scaffolding elements

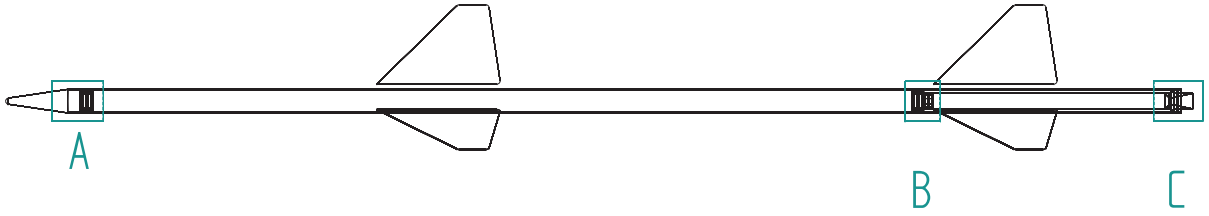

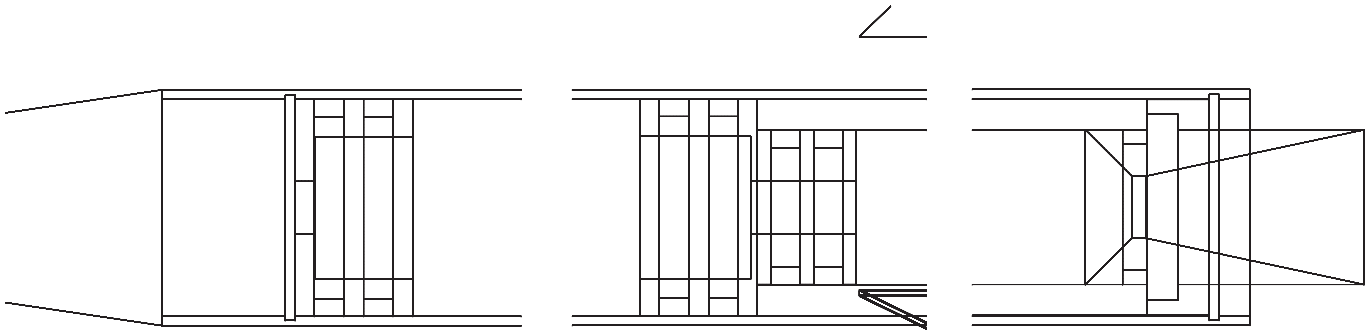

DETAIL A

DETAIL B

DETAIL C

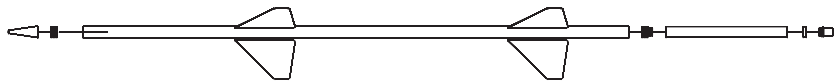

	NAME	DATE
DRAWN	Mike Grant	01/11/06
CHECKED		
ENG APPR		
MGR APPR		

UNLESS OTHERWISE SPECIFIED
DIMENSIONS ARE IN MILLIMETERS
ANGLES ±0.05°
2 PL ±0.01 3 PL ±0.005

Baneka Lightning Project
University of the Witwatersrand

TITLE: Rocket 1-B

SIZE	DWG NO	REV
A4	1	B

FILE NAME: Rocket.dft

SCALE:	WEIGHT:	SHEET 1 OF 8

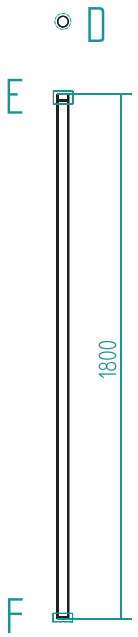

Body
1:20

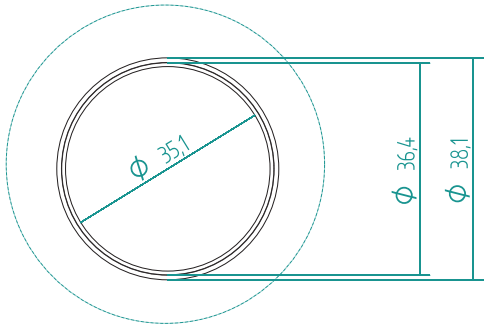

DETAIL D

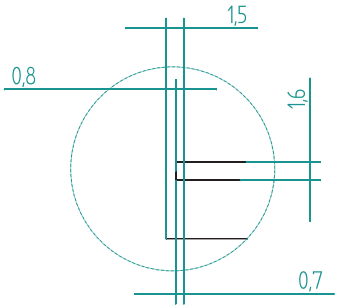

DETAIL G

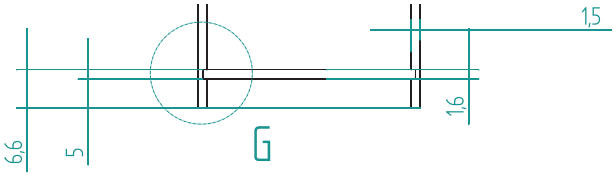

DETAIL F

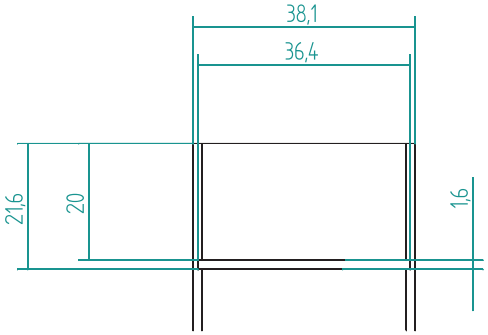

DETAIL E

Please construct from Aluminium 6063-T6 round tube

Two cuts for circlips at each end. It is important that the remaining material is no less than 0,8mm thick, so groove depth will vary with material tolerances.

	NAME	DATE
DRAWN	Mike Grant	01/11/06
CHECKED		
ENG APPR		
MGR APPR		

UNLESS OTHERWISE SPECIFIED
DIMENSIONS ARE IN MILLIMETERS
ANGLES ±0.05°
2 PL ±0.01 3 PL ±0.005

Baneka Lightning Project
University of the Witwatersrand

TITLE: Rocket 1-B

SIZE	DWG NO	REV
A4	1	B

FILE NAME: Rocket.dft

SCALE:	WEIGHT:	SHEET 2 OF 8

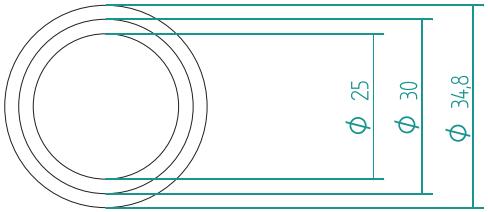

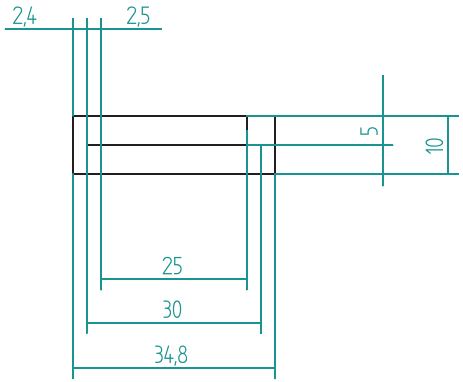

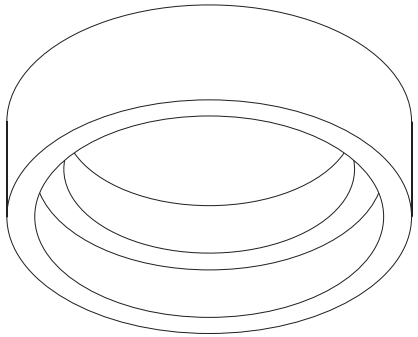

Thermal Insulator

1:1

Please construct from Phenolic liner from a solid rod.

Ensure a good fit with the nozzle and body parts.

	NAME	DATE
DRAWN	Mike Grant	01/11/06
CHECKED		
ENG APPR		
MGR APPR		

UNLESS OTHERWISE SPECIFIED
DIMENSIONS ARE IN MILLIMETERS
ANGLES ±0.05°
2 PL ±0.01 3 PL ±0.005

Baneka Lightning Project
University of the Witwatersrand

TITLE: Rocket 1-B

SIZE	DWG NO	REV
A4	1	B

FILE NAME: Rocket.dft

SCALE:	WEIGHT:	SHEET 3 OF 8

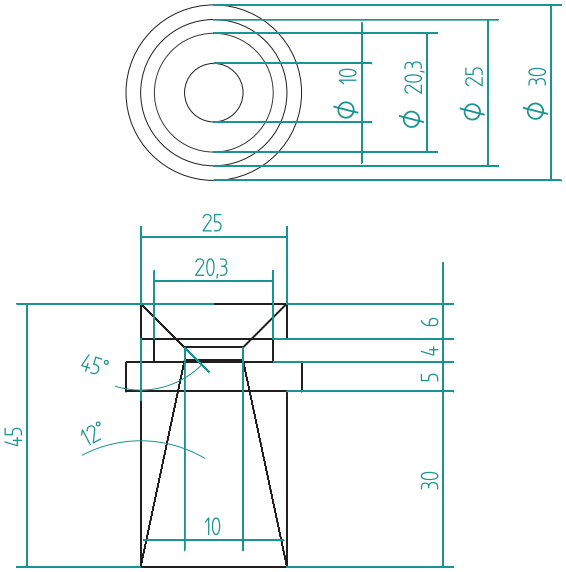

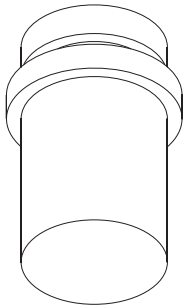

Nozzle
1:1

Please construct from high density graphite.

Please note that the angles are critical and should be turned to absolute maximum tolerances obtainable.

	NAME	DATE
DRAWN	Mike Grant	01/11/06
CHECKED		
ENG APPR		
MGR APPR		

UNLESS OTHERWISE SPECIFIED
DIMENSIONS ARE IN MILLIMETERS
ANGLES ±0.05°
2 PL ±0.01 3 PL ±0.005

Baneka Lightning Project
University of the Witwatersrand

TITLE: Rocket 1-B

SIZE	DWG NO	REV
A4	1	B

FILE NAME: Rocket.dft

SCALE:	WEIGHT:	SHEET 4 OF 8

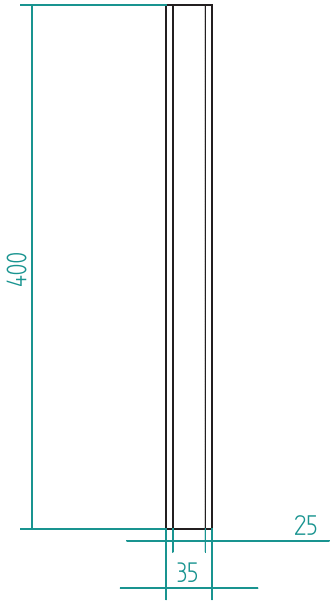

Grain
1:5

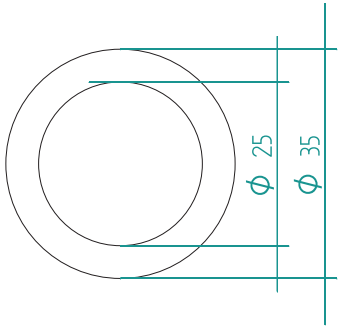

1:1

Please construct from high density polypropylene, with no additives (clear).

This part can be machined from solid rod or extruded provided density remains high.

	NAME	DATE
DRAWN	Mike Grant	01/11/06
CHECKED		
ENG APPR		
MGR APPR		

UNLESS OTHERWISE SPECIFIED
DIMENSIONS ARE IN MILLIMETERS
ANGLES ±0.05°
2 PL ±0.01 3 PL ±0.005

Baneka Lightning Project
University of the Witwatersrand

TITLE: Rocket 1-B

SIZE	DWG NO	REV
A4	1	B

FILE NAME: Rocket.dft

SCALE:	WEIGHT:	SHEET 5 OF 8

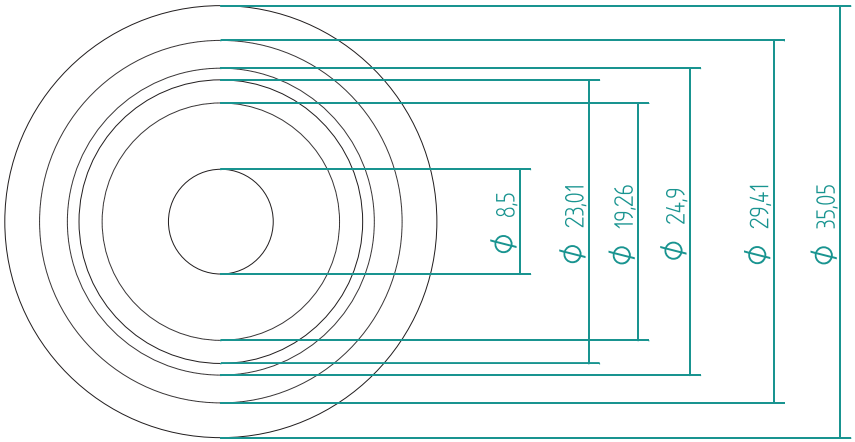

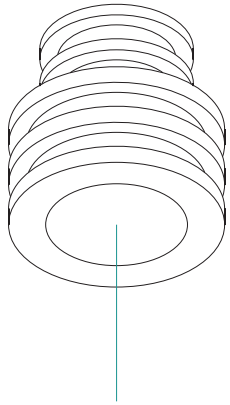

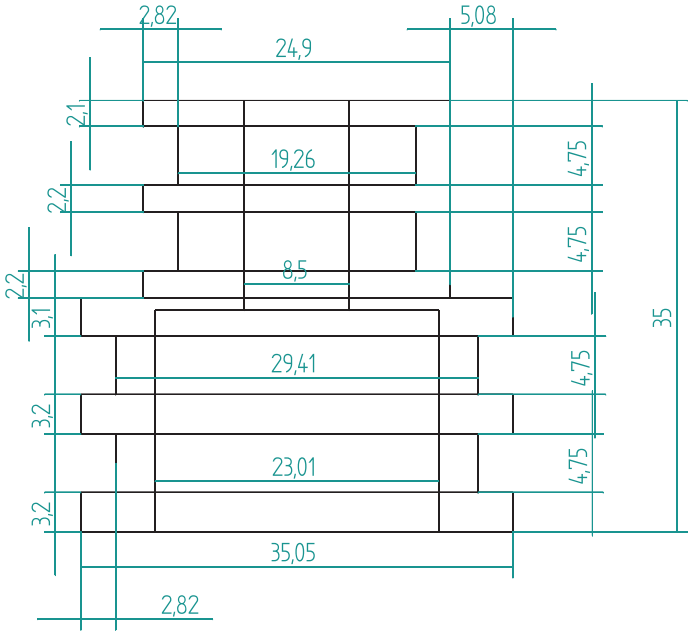

Injector
2:1

Please construct from Aluminium 6063 grade or better.

Please note that small diameter hole of 8.5 needs to be threaded with a 1/8" NPT thread from the wide side into the the smaller side, as indicated by the arrow above.

	NAME	DATE
DRAWN	Mike Grant	01/11/06
CHECKED		
ENG APPR		
MGR APPR		

UNLESS OTHERWISE SPECIFIED
DIMENSIONS ARE IN MILLIMETERS
ANGLES ±0.05°
2 PL ±0.01 3 PL ±0.005

Baneka Lightning Project
University of the Witwatersrand

TITLE: Rocket 1-B

SIZE	DWG NO	REV
A4	1	B

FILE NAME: Rocket.dft

SCALE:	WEIGHT:	SHEET 6 OF 8

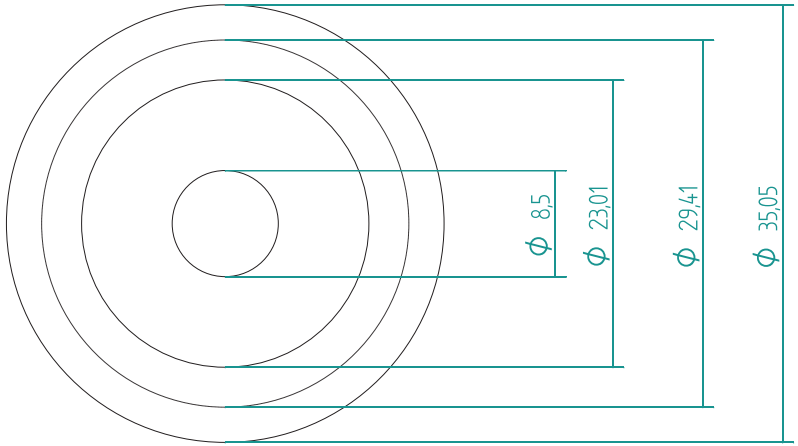

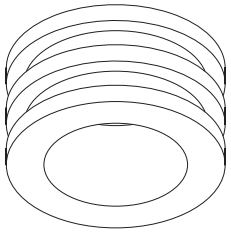

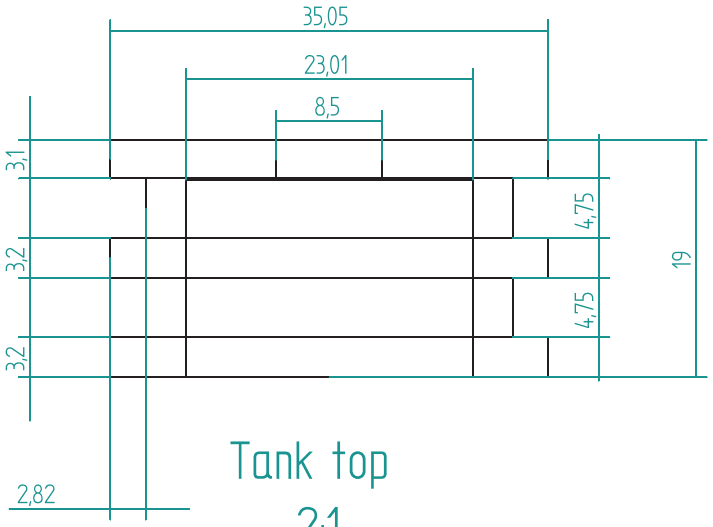

Tank top
2:1

Please construct from Aluminium 6063 grade or better.

Please note that small diameter hole of 8.5 needs to be threaded with a 1/8" NPT thread from the flat face into the cavity

	NAME	DATE
DRAWN	Mike Grant	01/11/06
CHECKED		
ENG APPR		
MGR APPR		

UNLESS OTHERWISE SPECIFIED
DIMENSIONS ARE IN MILLIMETERS
ANGLES ±0.05°
2 PL ±0.01 3 PL ±0.005

Baneka Lightning Project
University of the Witwatersrand

TITLE: Rocket 1-B

SIZE	DWG NO	REV
A4	1	B

FILE NAME: Rocket.dft

SCALE:	WEIGHT:	SHEET 7 OF 8

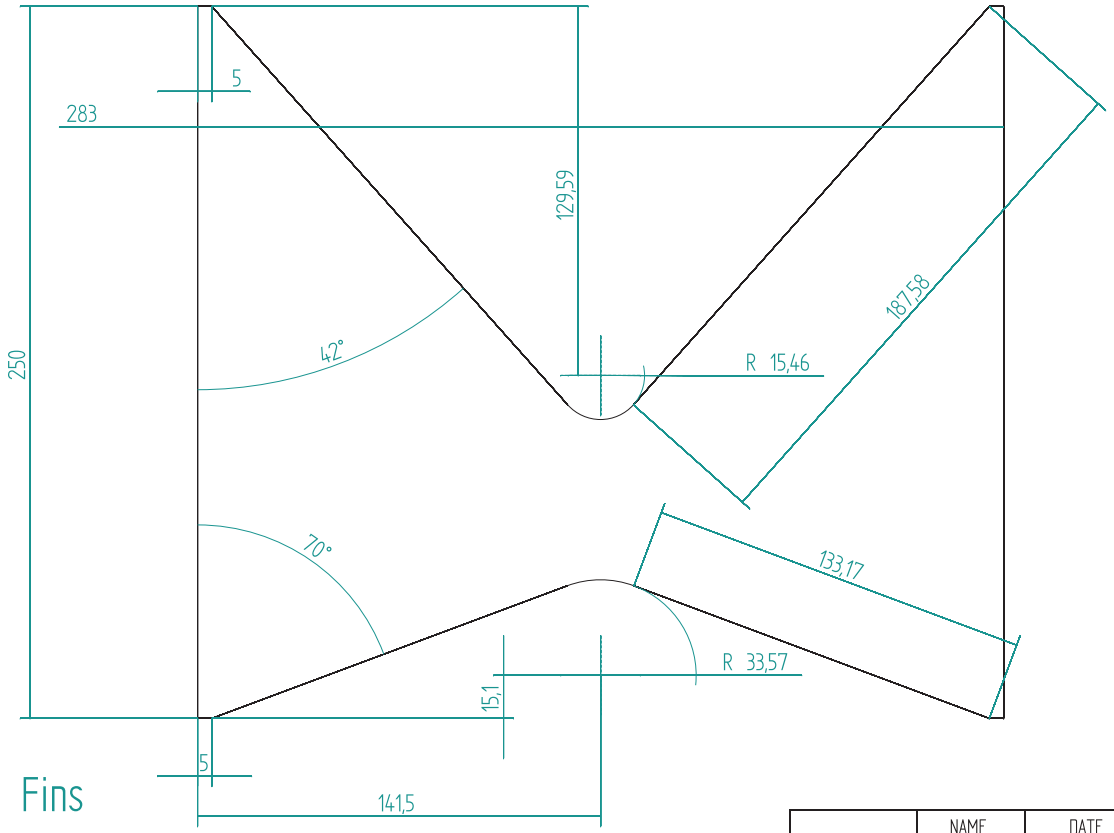

Fins

1:2

Please construct from Aluminium 6063-T6 1.5 mm thick.

This part should be laser cut.

	NAME	DATE
DRAWN	Mike Grant	01/11/06
CHECKED		
ENG APPR		
MGR APPR		

UNLESS OTHERWISE SPECIFIED
DIMENSIONS ARE IN MILLIMETERS
ANGLES ±0.05°
2 PL ±0.01 3 PL ±0.005

Baneka Lightning Project
University of the Witwatersrand

TITLE: Rocket 1-B

SIZE	DWG NO	REV
A4	1	B

FILE NAME: Rocket.dft

SCALE:	WEIGHT:	SHEET 8 OF 8

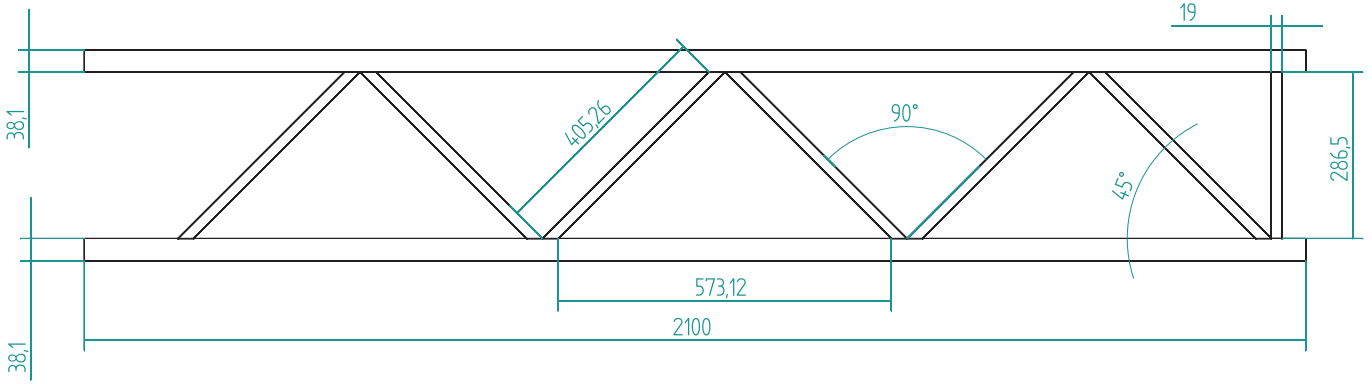

Scaffolding
1:10

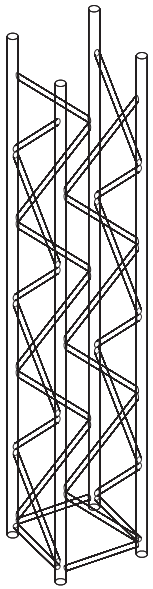

Tower Assembled

	NAME	DATE
DRAWN	Mike Grant	07/24/06
CHECKED		
ENG APPR		
MGR APPR		

UNLESS OTHERWISE SPECIFIED
DIMENSIONS ARE IN MILLIMETERS
ANGLES ±0.5°
2 PL ±0.0˙11 3 PL ±0.005

Baneka Lightning Project
University of the Witwatersrand

TITLE: Launch Tower

SIZE	DWG NO	REV
A4		

FILE NAME: Scaffolding.dft

SCALE:	WEIGHT:	SHEET 1 OF 2

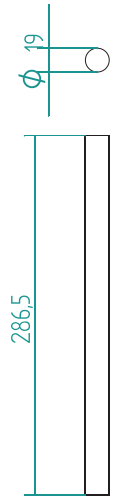

Horizontal Strut
1:5

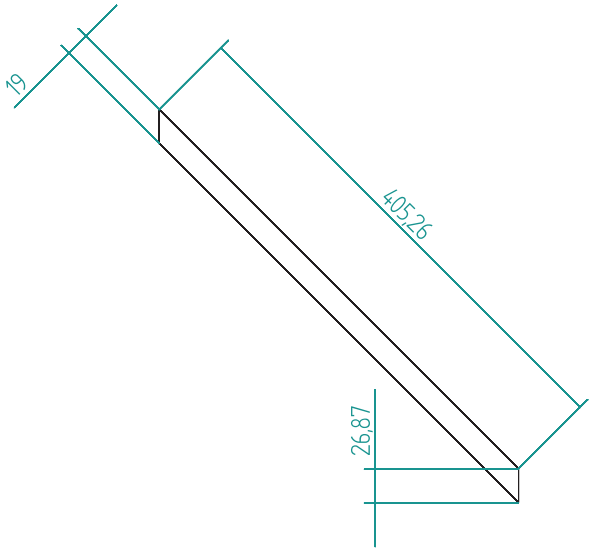

Diagonal Strut
1:5

	NAME	DATE
DRAWN	Mike Grant	07/24/06
CHECKED		
ENG APPR		
MGR APPR		

UNLESS OTHERWISE SPECIFIED
DIMENSIONS ARE IN MILLIMETERS
ANGLES ±0.5°
2 PL ±0.011 3 PL ±0.005

Baneka Lightning Project
University of the Witwatersrand

TITLE: Launch Tower

SIZE	DWG NO	REV
A4		

FILE NAME: Scaffolding.dft

SCALE:	WEIGHT:	SHEET 2 OF 2

	NAME	DATE
DRAWN	Mike Grant	07/24/06
CHECKED		
ENG APPR		
MGR APPR		

UNLESS OTHERWISE SPECIFIED
DIMENSIONS ARE IN MILLIMETERS
ANGLES ±0.5°
2 PL ±0.011 3 PL ±0.005

Baneka Lightning Project
University of the Witwatersrand

TITLE: Launch Tower

SIZE A4 | DWG NO | REV

FILE NAME: Scaffolding.dft

SCALE: | WEIGHT: | SHEET 3 OF 3

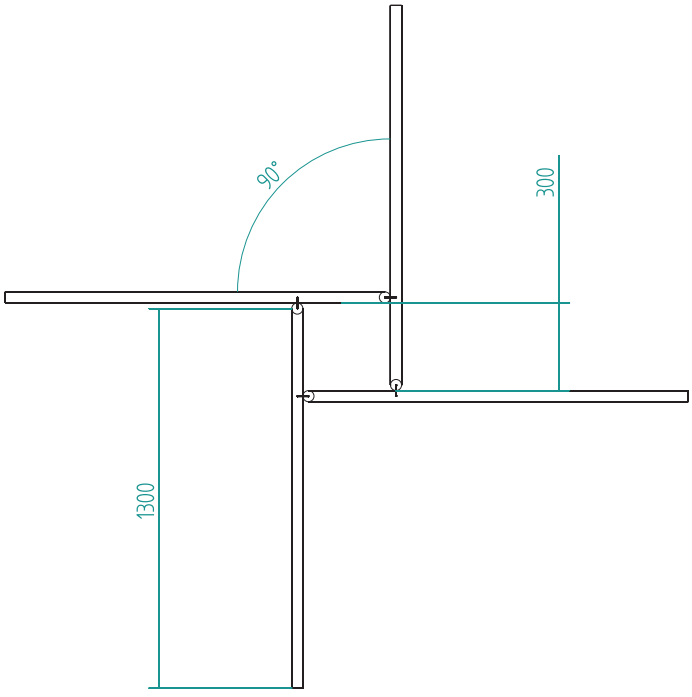

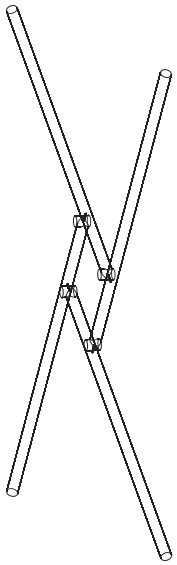

Base

LOW COST ELECTRIC-FIELD MILL: DESIGN, CONSTRUCTION AND TESTING

M D Grant, J M Garrard and K J Nixon

School of Electrical and Information Engineering, Lightning/EMC Research Group, University of the Witwatersrand, Private Bag 3, 2050, Johannesburg, South Africa

Abstract: A design for a low cost field mill is presented consisting of the supporting electrostatic theory and mechanical construction. The design of the measurement system consisting of filters, digitisation and transmission is also presented. The device is calibrated and the laboratory results are included. Finally electric field measurements of a storm are presented.

Key words: electrostatics, field mill, measurement system, optical isolation

H.2 INTRODUCTION

Early studies indicate that knowledge of the charge structure within clouds is key to understanding the lightning phenomenon. A means of measuring the electric field of the clouds has been sought and several mechanisms to measure electric field have been proposed, but few as successful as the field mill [2]. As its name implies the sensor "mills" the incident electric field and compares it to an arbitrary and usually earth referenced ground [3, 4].

Traditionally, field mills consist of a rotary shutter which modulates the incident field to the sensor electrodes, and thus field strength can be found through peak detection [3]. This approach requires the rotary shutter to be grounded, so that the electrodes could discharge to a satisfactory level near to the signal reference. This approach has several disadvantages including noise introduced from the grounding brushes, corrosion and wear effects [5].

The "back-to-back" field mill includes a second shielded mill which eliminates the need for the noisy grounding [5]. The second mill senses the field present on the motor and primary rotary shutter, and when compared to the charge measured on the primary sensor electrodes yields the electric field strength. However the mechanical complexity of a "back-to-back" mill significantly increases the cost of production.

The electrostatic theory is presented and then applied to the mechanical design. The design of the measurement circuit is discussed, followed by the calibration of the system and the results thereof.

Presented at the 2006 SAUPEC conference, Durban, South Africa [1]

H.3 ELECTROSTATICS

From Gauss' Law, the charge induced on a surface due to the presence of an incident electric field is given by [6]:

$$Q = \epsilon_0 \vec{E} \cdot A \tag{1}$$

Where:
Q : Surface charge [C]
ϵ_0 : Permittivity of free space [$C^2/N{\cdot}m^2$]
$\vec{E}$: Incident electric field [V/m]
A : Surface area [m^2]

Now the magnitude of the electric field, as modulated by the rotary shutter is given by:

$$E = E_f \cos\alpha \sin(\omega t) \tag{2}$$

Where:
E : E-Field exposed to the electrodes [V/m]
E_f : magnitude of the incident field [V/m]
α : Angle of the incident field [°]
ω : Angular velocity of the shutter [rad/s]

Hence the rate of change of the charge on the surface of an electrode is:

$$\frac{dQ}{dt} = E_f \cos\alpha \cos(\omega t)\, \omega A = i(t) \qquad (3)$$

Now if the surface is connected to an arbitrary reference through a resistor, then the potential between the surface and the reference is given by:

$$V = R\frac{dQ}{dt} \qquad (4)$$

However if the primary shutter has accumulated an nominal offset charge of Q_o coulombs. Then the charge on the sensor electrodes is:

$$Q_{\text{total}} = Q - Q_o \qquad (5)$$

From this, the charge inducted on the sensor electrodes by the electric field can be found when a charge has accumulated on the rotary shutter.

H.4 MECHANICAL DESIGN

A single rotary shutter and electrode combination is implemented since a "back-to-back" implementation is not feasible. *Figure H.1* illustrates the mechanical implementation.

H.4.1 *Sensor Electrode and Rotary Shutter*

From *Equation 1*, the amount of charge induced on an electrode is proportional to the surface area of the electrode. Since the field must be modulated by the rotary shutter, the maximum surface area of an electrode is half the cross sectional area of the shield can.

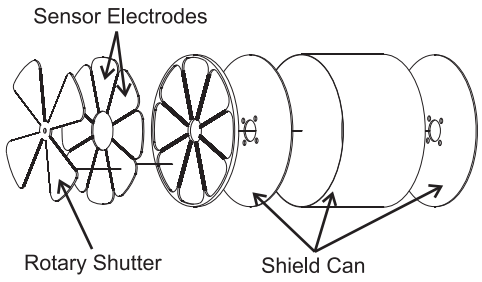

Figure H.1: Assembly diagram of field mill with labelled components

Since the aim is to induce a current from the sensor electrodes by modulating the electric field, then from *Equation 3* the rate of modulation is proportional to the angular velocity of the rotary shutter. Hence if the number of pairs of arms of the rotary shutter is increased then the rate of modulation of the electric field is increased by:

$$\omega_e = n\omega_r \qquad (6)$$

Where:
ω_e : Effective angular velocity [rad/s]
ω_r : Actual angular velocity [rad/s]
n : Number of arm pairs

Similarly the number of sensor electrodes needs to be increased as the number of arm pairs is increased. Thus the minimum number of sensor electrodes is twice the number of arm pairs.

H.4.2 *Fringing effects*

The electric field will be affected by the presence of conductors, this phenomenon is termed fringing. This plays a very obvious role when designing for the sensor electrodes and their location within the field mill.

If the sensor electrodes are too close to the shield can or rotary shutter then the fringing effects will reduce the magnitude of the modulated electric field. The same holds true if the sensor electrodes are too deeply recessed into the shield can. Ultimately the sensor electrodes must lie flush with the top of the shield can, with the rotary shutter just above the electrodes.

H.5 MEASUREMENT CIRCUIT

As detailed previously, measurement of the charge accumulated on the sensor electrodes is realised as a voltage measured across a resistor. An high input impedance stage of 200 kΩ is required to minimise the loss of sensitivity due to driving the signal into the input stage. The signal is then sampled by a microcontroller and then transmitted serially to a recording device.

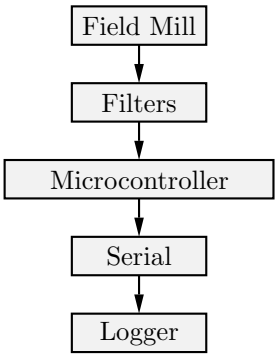

Figure H.2: Schematic diagram of the field mill and measurement system

H.5.1 *Signal conditioning*

As shown in *Figure H.3*, the voltage signal from the sensor electrodes is a sine wave with amplitude dependent on the incident electric field magnitude as predicted by *Equation 3*.

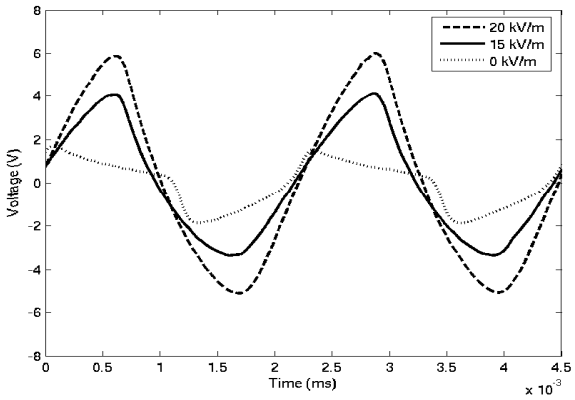

Figure H.3: Voltage waveform from sensor electrodes of field mill for different electric field magnitudes at the same separation distance

This signal must be buffered, amplified and filtered before the microcontroller can sample it. This is achieved by the circuit illustrated in *Figure H.4*. The signal is first buffered by high impedance FET amplifier, then amplified by a common small signal inverting op-amp. Finally the signal is rectified into a peak detect network.

H.5.2 *Data acquisition*

Central to the measurement system is a PIC16F877 microcontroller from MicroChip [7]. The microcontroller samples the analogue output from the mill and transmits the sample and a checksum along a serial link to a recording device. *Figure H.2* illustrates the location of the microcontroller within the measurement system.

The checksum was calculated using a bit by bit cyclic redundancy check (CRC) algorithm. As illustrated in *Figure H.5*, a four bit polynomial is used as there are four bits for a checksum in the two byte serial packet sent from the microcontroller to the recording device.

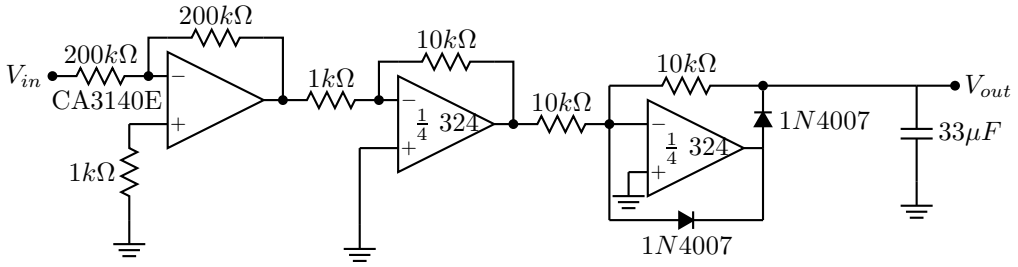

Figure H.4: Active filter and rectification circuit for the sensor electrode signal to drive the ADC module of the microcontroller

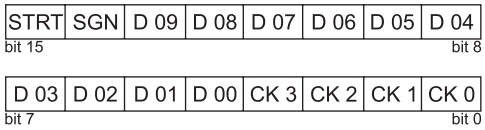

bit 15	STRT	Start bit always read as a 1
	SGN	Sign bit ($1 = \ominus, 0 = \oplus$)
bit 13	D 09	
	⋮	Data bits
bit 4	D 00	
bit 3	CK 3	
	⋮	Checksum bits
bit 0	CK 0	

Figure H.5: Two byte serial packet contents

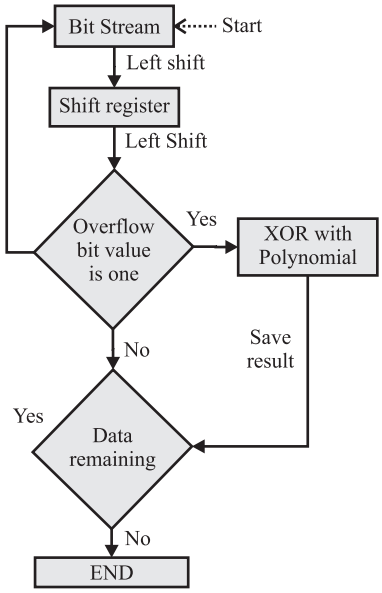

Figure H.6: CRC Algorithm implemented on the Microcontroller

The CRC is calculated by dividing the data stream by a pre-determined constant. This division is implemented by an XOR operation, the remainder of which is sent as the four bit checksum [8]. *Figure H.6* illustrates the implemented CRC algorithm.

H.5.3 *Optical Isolation*

The primary use of the field mill will be as a means of pre-lightning-strike detection, and hence there is a possibility that lightning might terminate on the field mill. Thus galvanic isolation of the field mill from the recording equipment is required. Ideally the recording equipment should be housed several hundred metres away from the field mill. Transmission of the digital signal through a fibre optic link solves both the isolation and separation problems.

The output of the fibre diodes is in TTL voltage levels which then needs to be increased to RS-232 voltage levels. This is easily achieved through a discrete semi-conductor (MAX-232). However fibre optic diodes are designed for data rates well in excess of the relatively slow serial bauds. As

a result the diode on time is much longer than commonly used in fibre transmissions [9]. Thus the diodes need to be driven with less than 100 mA from a stable current source.

H.6 CALIBRATION

The electric field sensing system was calibrated with an electric field generated by an HV-DC generator. The generator used is a single stage Cockroft-Walton, that generates a DC voltage twice that of the AC source used to drive the generator [10]. A maximum DC voltage of 20 kV is used in the calibration. Calibration is performed between to large parallel plates driven by the HV-DC supply. The electric field between the two plates is described by:

$$E = V/d \tag{7}$$

Where:
E : Electric field [V/m]
V : Voltage between the plates [V]
d : Distance between the plates [m]

From *Equation 7*, the magnitude of the electric field used to calibrate the mill can by varied by adjusting the applied voltage or the distance between the plates. *Figure H.7* details the relationship between the incident electric field magnitude and the field mill output.

As expected, the gradient of the tests differ depending on the plate separation distance. This is due to fringing between the charged plate and surrounding conductors at large separation distances. The calibration curve that is used is based on the data set from the shortest separation distance as this exhibits the least amount of fringe losses [6].

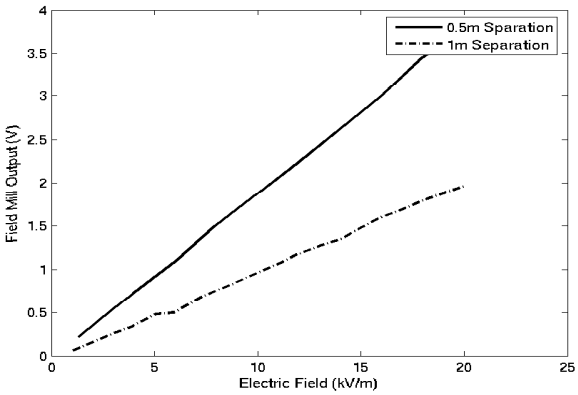

Figure H.7: Electric field magnitude to field mill output for different separation distances for laboratory calibration

H.7 RESULTS

An electrical storm passed over the constructed field mill on the 7th of January 2006. Spikes corresponding to flashes is clearly visible, as is pre-strike electrical activity.

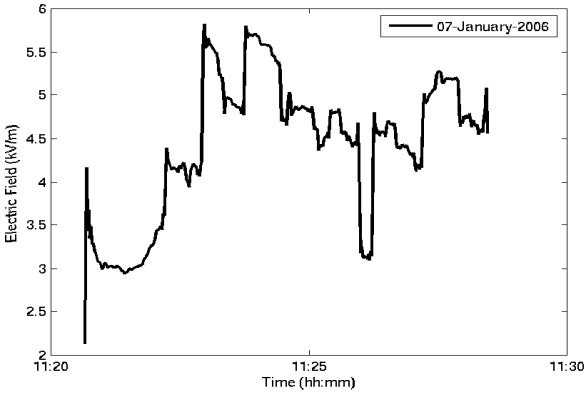

Figure H.8: Electric field measurements of a high veld electrical storm

H.8 CONCLUSION

A design for a low cost field mill has been presented. The supporting electrostatic theory that explains the operation of the field mill has been investigated. The mill and supporting electronics has been constructed and tested. Calibration results confirm the expected behaviour of the mill. Electric field measurements of a high veld storm were obtained and presented.

ACKNOWLEDGEMENTS

The authors would like to thank Eskom for their support of the Lightning/EMC Research Group through TESP. They would also like to thank the Department of Trade and Industry (DTI) for THRIP funding and to thank the National Research Foundation (NRF) for direct funding of the research group.

References

[1] M. D. Grant, J. Garrard, and K. J. Nixon. Low cost electric-field mill: Design, Construction and Testing. In *Proceedings of the 2006 Southern African Universities Power Engineering Conference*. Durban, South Africa, Jan. 2006.

[2] B. Schonland. *The flight of thunderbolts*. Amen house, London, England: Oxford University Press, 1950.

[3] P. Zimmermann. Fieldmill Voltmeter MK 2. *http://freespace.virgin.net/paul.z/Electronic/fieldmill1.htm*. Last accessed July 31, 2006.

[4] V. Rakov and M. Uman. *Lightning: Physics and Effects*. The Edinburgh Building, Cambridge CB2 2RU, England: Cambridge University Press, 2003.

[5] J. C. Instrumentation. Introduction to Electrostatics: Section 3. *http://www.jci.co.uk/Electrostatics/Wshop-03.2.pdf*. Last accessed July 31, 2006.

[6] R. A. Serway, R. J. Beichner, and J. W. Jewett. *Physics for Scientists and Engineers*. 6277 Sea Harbour drive, Orlando, FL 32887-6777, USA: Saunders College Publishing, fifth ed., 2000.

[7] MicroChip Technology Inc. *http://www.microchip.com*. Last accessed July 31, 2006.

[8] W. H. Press, S. A. Teukolsky, W. T. Vetterling, and B. P. Flannery. *Numerical Recipes in C*. Cambridge University Press, 2002.

[9] A. Technologies. Low cost miniature fibre optic components. *http://www.agilent.com*. Last accessed July 31, 2006.

[10] E. Kuffel, W. Zaengl, and J. Kuffel. *High Voltage Engineering: Fundamentals*. Linacre House, Jordan Hill, Oxford OX2 8DP, England: Newnes, second ed., 2000.